The procoagulant effects of extracellular vesicles derived from hypoxic endothelial cells can be selectively inhibited by inorganic nitrite.

Cass Whelan[1], Nicholas Burnley-Hall[2*], Keith Morris[1], D. Aled Rees[3], Philip E. James[1].*

[1]Cardiff School of Sport & Health Sciences, Cardiff Metropolitan University, Cardiff, UK, CF5 2YB

[2]School of Medicine, Cardiff University, Cardiff, CF24 4HQ, UK.

[3]Neuroscience and Mental Health Research Institute, School of Medicine, Cardiff University, Cardiff, UK, CF24 4HQ

Running title: Procoagulant effects of hypoxic endothelial cell-derived vesicles

Correspondence address and request for reprints to: Professor Philip E. James

Cardiff School of Sport & Health Sciences, Cardiff Metropolitan University, Cardiff, UK, CF5 2SG

Email: pjames@cardiffmet.ac.uk Telephone: +44 02920 417129

*Authors contributed equally to this manuscript.

Essentials

- Endothelial-derived extracellular vesicles (EVs) are elevated in cardiovascular disease.
- EV produced following a hypoxic insult exhibit increased tissue factor and have reduced levels of tissue pathway factor inhibitor in comparison to normoxia-derived EVs.
- Endothelial-derived EVs produced under hypoxic conditions demonstrate increased pro-coagulant behaviour in in vitro assays including fibrin polymer formation following stimulation with thrombin, platelet activity and the clot microstructure.
- This pro-coagulant effect of hypoxia-derived EVs is abrogated by pre-treatment of endothelial cells in hypoxia with inorganic nitrite.

Key words: Extracellular vesicles, nitrite, coagulation, thrombosis, haemostasis

Abstract

Background: Extracellular vesicles (EVs) derived from endothelial cells are elevated in cardiovascular disease and promote inflammation and coagulation. Hypoxia is often a key feature and is itself a potent stimulator of increased EV production. Inorganic nitrite (NO_2^-) has beneficial and protective effects that are enhanced in hypoxia.

Objectives: Investigate the impact of hypoxia on the functional capacity of EV derived from endothelial cells under hypoxia, and assess whether pre-treatment of endothelial cells with NO_2^- can alter EV function.

Methods: Differential ultracentrifugation was used to isolate EV from the cultured endothelial cell line HECV (CEV), and from primary human umbilical cord derived endothelial cells (PEV), with time-resolved fluorescence used to assess EV protein composition. Clot formation was induced by thrombin and calcium in two assays; using an Alexa Fluor 594 human fibrinogen conjugate assay and standard turbidometry. Platelet aggregation was determined using multiple electrode aggregometry. Scanning electron microscopy was used to visualise fibrin clots.

Results: Hypoxia exposure (1% O_2) significantly increased CEV production in comparison to normoxia (21% O_2) (1825±72 EVs/cell vs 117±9 EVs/cell, $p<0.001$, respectively) but had no effect on CEV mean size (221±6 nm vs 203±4 nm, $p>0.05$). Hypoxia-derived PEVs contained significantly more tissue factor than normoxia-derived EVs (Relative Fluorescence Units (*RFU*) =7666±1698 vs 5958±1644, $p<0.001$, respectively) and less tissue factor pathway inhibitor (*RFU*=9799±2353 vs 19723±2698, $p<0.05$). Hypoxia significantly increased CEV induced fibrin polymer formation compared to normoxia (% area =46.98±0.97 vs 36.36±0.72, $p<0.05$). Pre-treatment of endothelial cells with NO_2^- in hypoxia abrogated this effect (% area=15.70±1.99, $p<0.001$). Hypoxia derived CEV non-significantly increased the maximum clot formed, shortened time to max clot, and increased time to clot lysis by turbidometry. ADP-mediated platelet aggregation was significantly elevated with PEV derived from hypoxia compared to normoxia (888.0±32.2 AU*min vs 671.5.2±28.3 AU*min, $p<0.01$). This was abrogated by pre-treatment of hypoxic endothelial cells with NO_2^- (716.5±744.3 AU*min, $p<0.001$).

Conclusions: Hypoxia-derived PEVs and CEVs exhibit increased procoagulant activity compared to normoxia-derived EVs, which we confirm to be mediated by an imbalance of

TF/TFPI. Pre-treatment of endothelial cells with NO_2^- reduces the pro-coagulant activity of EVs via a mechanism that is Hypoxia-inducible factor 1 (HIF-1) dependent, but independent of TF/TFPI.

Abbreviations

Extracellular vesicles (EVs)

Primary Human Umbilical Vein derived Endothelial Cells (HUVEC)

Human Vascular Endothelial Cell Line (HECV)

Primary HUVEC EVs (PEVs)

Cultured HECV EVs (CEVs)

Hypoxia-inducible factor 1 (HIF-1)

Nitrate (NO_3^-)

Nitrite (NO_2^-)

Nitric oxide (NO)

Nanoparticle tracking analysis (NTA)

Sodium nitrite ($NaNO_2$)

Serum-free medium (SFM)

Time-resolved fluorescence (TRF)

Tissue factor (TF)

Tissue factor pathway inhibitor (TFPI)

Von Willebrand factor (vWF)

Introduction

Extracellular vesicles (EVs) are defined as membrane-bound, submicron particles released by multiple cell types [1]. Increased EV production has been shown in a plethora of disease states, where the bioactive cargo EVs harbour is typically reflective of the stimuli which triggered their release from the parent cell [2]. Elevated levels of EV have been found in cancer [3–5], neurodegenerative disorders [6–9], and cardiovascular disease [10–12]. Endothelial cell derived EVs possess surface markers specific to endothelial cells including CD144 and CD62E [13,14] and express tissue factor, suggesting a role in augmenting the coagulation cascade [15]. When oxygen supply is limited to a particular tissue region, such as in instances of acute hypoxia or ischaemia during trans-ischaemic attack, myocardial infarction, or stroke, the number of EVs released from endothelial cells increases significantly [16,17] which then re-enter the normal circulation. Under these conditions, increased stability of hypoxia inducible factor (HIF) 1-α when O_2 is below 2% is responsible for the transcription of various genes involved in angiogenesis and inflammation [18,19], and as shown by our group and others, takes a central role in inducing increased endothelial derived- EVs [19,20]. These EVs exhibit markedly altered RNA and protein composition, although their role in inducing a downstream pro-coagulative state remains uncertain [21].

Hypoxia exposure of endothelial cells can reduce the expression of thrombomodulin and tissue factor pathway inhibitor (TFPI) and increase plasminogen activator inhibitor-1 expression, resulting in accelerated thrombin activity and stability of fibrin clots [22-24]. There is also accumulating evidence that has shown EVs derived from hypoxic conditions have increased pro-coagulant properties, including elevated tissue factor (TF) activity, thrombin generation and promotion of fibrinogenesis [25-28].

Nitrite (NO_2^-) is capable of eliciting vasoprotective effects via its chemical reduction to nitric oxide (NO) or other NO_x species, which is greatly augmented in hypoxia [29]. Endogenous NO_2^- regulates hypoxic vasodilation via its reduction to NO, matching blood flow and O_2 supply to the metabolic demand under hypoxic conditions [30]. Exogenous NO_2^- (applied via dietary nitrate supplement) reduces mean arterial blood pressure by ~5-10mmHg and can reduce patient derived platelet aggregation [31,32]. NO itself is known to modulate the cellular response to hypoxia by preventing the stabilization of HIF-1α via an increase in prolyl hydroxylase-mediated degradation [33]. Its role in modulating endothelial derived EV is less clear. Impaired endogenous NO production in primary endothelial cells (HUVECs) has

been shown to increase EV formation [34]. Furthermore, we have previously shown that NO_2^- derived NO is capable of reducing hypoxia-mediated EV production in endothelial cells in a HIF-1α dependant manner [20]. Although the effect of NO_2^- on vascular homeostasis is already established [35-37], its influence on the pro-thrombotic function of hypoxia-derived EVs has not been evaluated.

The aim of this study was to firstly assess the coagulation capacity of endothelial-derived EVs generated under hypoxic conditions and identify the pathways involved, and secondly, investigate whether pre-treatment of endothelial cells with inorganic NO_2^- was able to modulate the pro-coagulant capacity of EV produced.

Methods

Cell Culture

The human vascular endothelial cell line (HECV) is a clone line previously purchased from Interlab (Milan, Italy) and routinely used in our laboratory. Cells were maintained in 90% Dulbecco's Modified Eagle Medium (DMEM) (PAA Laboratories, UK) supplemented with 10% (v/v) foetal bovine serum (FBS) (PAA Laboratories, UK) and 1% streptomycin/penicillin (Invitrogen, UK). Cells were incubated at 37ºC in 5% CO_2. At approximately 90% confluence cells underwent passage using Trypsin-EDTA (Invitrogen, UK) and exhibited a "cobble-stone"-like appearance typical of endothelial cells. HECVs were exposed to hypoxia using an InVivo2 hypoxic workstation 400 (Baker Ruskinn, UK) and maintained at 1% O_2 for 24 hours. The oxygen concentration was monitored using an i-CO2N2 gas mixing system (Baker Ruskinn, UK). 1% O_2 was chosen specifically because it is equivalent to a pO_2 ~7.6mmHg and in vitro model of ischaemia, as we and others have utilised extensively [20].
Sodium nitrite ($NaNO_2$) was administered simultaneous to hypoxic exposure, or in normoxia as a control, to endothelial cells at a final concentration of 30µM, which is a supra-physiological dose based upon the previously established maximal inhibition effect of NO_2^- on EV production [20].

HUVECs were isolated directly from umbilical cords, as previously described, with minor modifications [38]. Human umbilical cords were obtained from the Delivery Suite, Cardiff and Vale University Health Board Trust. Ethical approval was obtained from a Research Ethics Committee (REC) (REC reference: 14/NW/1459). Umbilical cords were cut to approximately 15 cm, avoiding any damage from clamps used during birth. Cords were washed with 0.9% saline to remove excess blood and clots. The vein was located and washed through with saline until the solution ran clear. One end of the cord was clamped, and collagenase (1 mg/mL) was infused into the umbilical vein, before incubation at room temperature for 30 minutes. The collagenase solution was removed and placed into a centrifuge tube, gently squeezing the cord to ensure complete cell detachment. The resulting solution was then centrifuged at 300 x *g* for 5 minutes to pellet HUVECs. HUVECs were resuspended in complete M199 medium (Gibco, ThermoFisher Scientific, UK), before being plated onto cell culture plates or flasks pre-coated with 1% gelatin. Cells were left to adhere overnight, before medium was changed after 12-18 hours in order to remove erythrocyte contamination. HUVECs were counted manually using a

haemocytometer. HUVECs were exposed to hypoxia using to an InVivo2 hypoxic workstation and $NaNO_2$ administered as for HECV (above).

EV isolation

HUVECs and HECVs were grown to confluence and incubated under their specified conditions in serum-free media (SFM) for 24 hours prior to EV isolation. Cell-conditioned culture medium was then removed and subjected to a differential ultracentrifugation method, as described previously [39]. Briefly, cell media (typically 30mLs) was centrifuged at 300 x g for 5 minutes to remove any detached cells in suspension. This supernatant was taken and subjected to a second centrifugation at 15,000 x g for 15 minutes at 4°C to pellet any cellular debris or apoptotic bodies. This supernatant was then isolated and subjected to a third and final ultracentrifugation at 100,000 x g for 60 minutes at 4°C in order to pellet EVs (typically ~100µL). This pellet was then resuspended in 750µL 1x PBS, which had been filtered with a 0.22 µm filter (Millex®, Merck Millipore, Ireland).

Nanoparticle Tracking Analysis

The concentration of PEVs and CEVs was determined using nanoparticle tracking analysis (NTA, NanoSight LM10 system, UK) as we have described previously [40]. NTA is a laser illuminated microscopic technique equipped with a 642 nm laser and a high sensitivity digital camera system (OrcaFlash2.8, Hamamatsu, NanoSight Ltd) that determines the Brownian motion of individual nanoparticles in real-time to assess size and concentration. Sixty-second videos were recorded, and particle movement was analysed using NTA software (version 2.3). Shutter speed was fixed at 30.01 ms and camera gain to 500. Camera sensitivity and detection threshold were typically (11–14) and (4–6), respectively. PEV and CEV samples were diluted in EV-free sterile water (Fresenius Kabi, Runcorn, UK) and the EV concentration was normalised prior to application to in vitro functional assays.

Characterisation of EVs

Time-resolved fluorescence coupled with a modified ELISA technique was used to assess both the surface protein and content of the isolated PEVs derived from various conditions, as described previously [40]. PEVs were loaded onto a high protein binding 96-well plate (Greiner Bio-One, Germany) overnight at 4°C, before non-specific sites were blocked with 1% BSA (R&D Systems) for two hours. PEVs were permeabilised using a RIPA lysis buffer (Santa Cruz, CA, USA) to allow analysis of intra-vesicular proteins. PEVs were incubated

overnight with mouse anti-human antibodies for typical EV markers CD9, ALIX, and TSG101, and for typical endothelial markers CD144 (VE-Cadherin), Von Willebrand factor (vWF), tissue factor (TF), and TFPI, (all Abcam, Cambridge, UK) overnight at 4°C. Markers were detected using a biotinylated anti-mouse IgG secondary antibody (PerkinElmer, Buckinghamshire, UK) and a streptavidin:europium conjugate (PerkinElmer, Buckinghamshire, UK) and measured by time-resolved fluorescence (delay time: 400 µs, measurement window: 400 µs) using a BMG Labtech CLARIOstar.

Fluorescent Fibrin Polymer Formation

The Alexa Fluor 594 human fibrinogen conjugate (Thermo Fisher Scientific, USA), with absorption and emission maxima of 592 nm and 618 nm respectively, was used to visualise the formation of fibrin-based polymers in real time, adapted from a method previously described [41] and reviewed [42,43]. Thawed human plasma was introduced to fluorescent fibrinogen at a final concentration of 5% and endothelial CEVs at a concentration of $1x10^9$ EVs/mL in 100µL consecutively. Simultaneously, a Hanks Based Salt-Solution (HBSS) containing 5U/mL thrombin (Merck, USA) and 200mM calcium chloride ($CaCl_2$) (Beckman Coulter, UK) was added to the plasma containing CEVs and fluorescent fibrinogen, for a final concentration of 0.5U/mL thrombin and 20mM $CaCl_2$ in 100µL. The introduction of HBSS to plasma represented time point 0. A high concentration of thrombin catalyses the conversion of fibrinogen to fibrin. 20µL of this mixture was placed on a glass microscope slide and covered with a coverslip. Fibrin polymer formation was monitored over time at 100x magnification on a Nikon-80i microscope (Nikon, Japan) and captured using Volocity-64x software (a typical time-course is shown in supplementary material – Figure 1). Maximal clot formation was reflected from images captured and measured at 15 minutes, where beyond 15 minutes, only a slight increase in fluorescence occurs [41]. Controls were lacking the addition of CEVs. Results were analysed on Adobe Photoshop (Adobe Inc., California, USA) from 16 individual points of interest on each single repetition, where 'fibrin percentage area' represents a pixel-by-pixel coverage of the image by fibrin polymers versus total pixels, where 14.42 pixels represents 1µm. The number of fibrin polymers intersecting at a junction was determined by the number of strands per junction and is a measure of fibrin clot formation.

Turbidometry

Turbidometry was employed to analyse clot formation and lysis. The assay was originally developed by Professor Ajjan's group at Leeds University Hospital [44,45] and modified as follows. EVs from cells subjected to normoxic and hypoxic conditions (+/- nitrite), respectively, were added to human plasma (a pooled standard that had originated from healthy control subjects) at a concentration of $1x10^9$ EVs/mL in 100µL before the addition of thrombin and calcium at a final concentration of 0.03U/mL thrombin, 7.5mM $CaCl_2$, and 83.2ng/mL tissue plasminogen activator (tPA) in a total assay volume of 150µL. Samples were prepared in triplicate. Absorbance readings at 340 nm were recorded using a CLARIOstar Plus 96 well plate reader (BMG Labtech, England) at 37°C for up to 60 min. From the absorbance profile over time, the maximal clot formed was measured from the peak absorbance, the rate of clot formation calculated from baseline to peak absorbance over time, rate of clot lysis calculated from the peak to baseline return over time, and time to 50% lysis. These were compared to a paired control consisting of plasma with no EVs added.

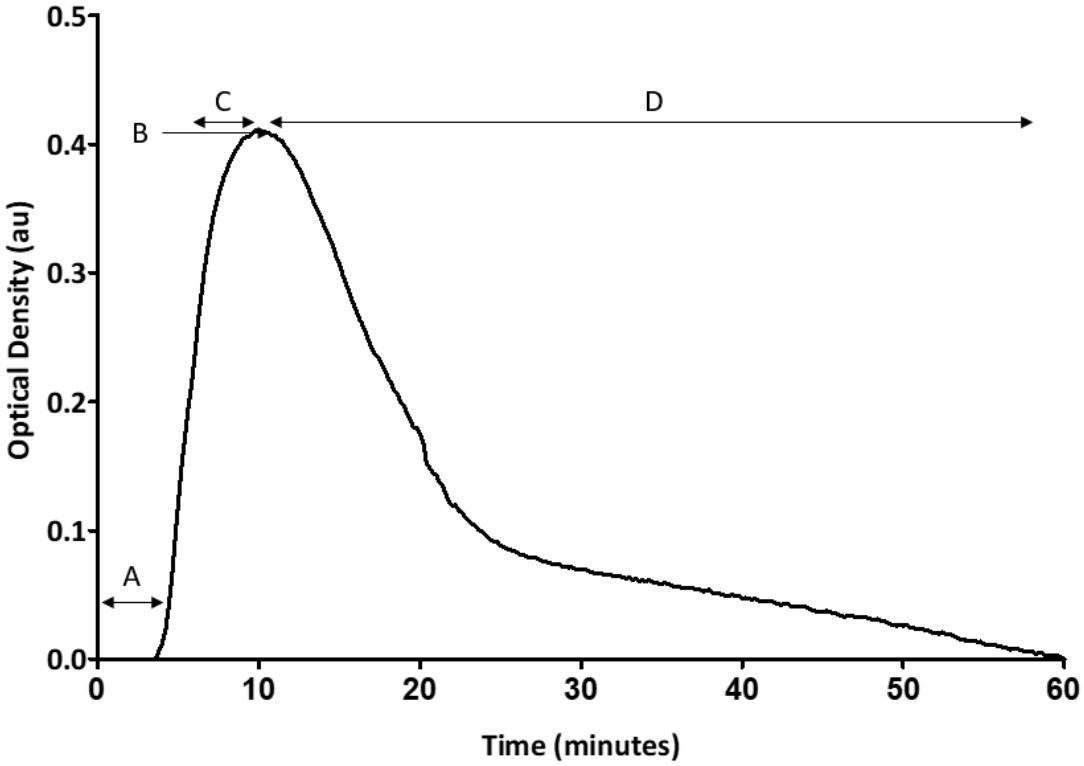

Figure 1. **Typical coagulation trace using thrombin as the activator and tPA as the lysis initiator in platelet free plasma without the addition of EVs.** A = the delay in clot formation (seconds). B = the maximum optical density (au), the maximum strength of the clot. C = clot formation, from which the time taken for clot formation to reach its maximum point can be calculated (minutes). D = Clot lysis, the rate of clot lysis can be calculated (minutes). The graph demonstrates clot formation and lysis is complete within 1 hour.

Platelet aggregation

Whole blood (300µL) of healthy volunteers collected into a hirudin BD Vacutainer ® was diluted 1:1 with EVs in PBS (final concentration: $2x10^8$/mL) and preheated to 37°C in a single use test cell for 3 minutes for Multiplate® platelet aggregometry. Samples were continuously homogenised using a Teflon coated stirring bar at 1000 rpm. Platelet activation was then initiated by the addition of either ADP (20µL, final concentration 6.5µM) or TRAP (Thrombin receptor activating peptide, 20µL, final concentration 32µM) (Roche Diagnostics Ltd, Switzerland). An example of ADP and TRAP aggregation curves is shown in Figure 2. An increase in electrical impedance was recorded for 6 minutes, with timing based on Multiplate® test parameters that are required to assess velocity of aggregation, maximum aggregation, and area under the curve (AUC), and expressed as arbitrary aggregation units.

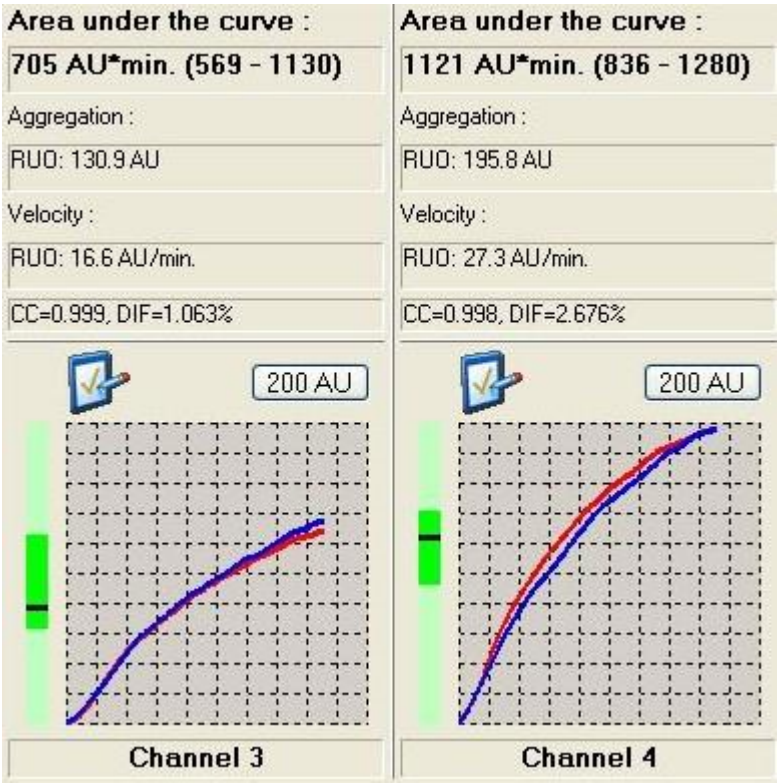

Figure 2. Representative aggregation curves for ADP and TRAP. Whole blood was incubated, before platelets were stimulated with either ADP (left) or TRAP (right). Aggregation units calculated as area under the curve after 6 minutes (impedance:time).

Fractal Dimension and Clot Formation Time

The haemorheological gel point technique has been previously described [46,47]. Briefly, blood was loaded into a double concentric measuring geometry on a controlled stress rheometer, AR-G2 (TA Instruments, New Castle, DE, USA). Small amplitude oscillatory

shear measurements were performed at test frequencies (2 Hz, 0.93 Hz, 0.43 Hz and 0.2 Hz) with a peak stress amplitude of 0.03 Pa. This allowed the phase angle (δ) (the difference between the applied stress and measured strain) to be determined. The method detects the Gel Point (GP) by measuring the difference in δ at the varying frequencies with respect to time. GP represents the formation of the incipient blood clot; the first point at which the fluid transitions to a solid. GP allows quantification of how the fibrin clot is organised using fractal analysis, to determine the clot's fractal dimension (d_f), which was normalised to the PBS control. In addition, measurement of the GP provides a measure of clot formation time (T_{GP}) which is the time taken to form the clot.

Blood from healthy volunteers was taken into 3.2% sodium citrate vacutainers®, aliquoted into 7mL vials and incubated at 37ºC with PEVs (final concentration $2x10^8$/mL) for 15 minutes. Citrated blood samples were then re-calcified by adding 334µL 0.2M calcium chloride, before being immediately loaded into the rheometer. The process from recalcifying the blood to initialization of the measurement was performed in less than 60 seconds. Samples were allowed to run for sufficient time to reach the GP, never exceeding more than 10 minutes.

Thrombin generation assay

Thrombin activity was assessed using the Thrombin activity assay kit (Abcam, Cambridge, United Kingdom). The assay was undertaken as per the manufacturer's instructions. Briefly, a set of thrombin standards was prepared, before plasma isolated from the blood of healthy volunteers was diluted and added to the microplate. PEVs were added to plasma samples (final concentration $2x10^8$/mL) and incubated for 1 hour at 37°C, before a reaction mix (containing the fluorogenic thrombin substrate and buffer) was added to both plasma and standard wells. Fluorescence was measured at Ex/Em = 350/450 nm every 3 minutes for 60 minutes at 37°C. Following completion of this incubation, two time points were chosen within the linear portion of the time course to calculate the change in fluorescence and thus Thrombin activity. This change in fluorescence was then compared to a standard curve in order to calculate ng of Thrombin, allowing thrombin activity to be expressed as ng/mL.

Scanning electron microscopy

Scanning electron microscopy was used to visualise fibrin clots and the influence of PEVs in whole blood. Fibrin clots were formed at 37°C for 2 hours (due to correlations between

gelation time and final clot structure) by adding $CaCl_2$ (20mM). Clots were washed 3 times with sodium cacodylate buffer (0.2M), before being fixed in 2% glutaraldehyde in PBS (v/v) for 1 hour at room temperature. Clots were subjected to dehydration through graded ethanol (30-100%), before being fixed using hexamethyldisiazane. Finally, the sample was splutter coated with gold, and imaged using a Hitachi Ultra-high resolution FE-SEM S-4800.

Statistics

Data were analysed using GraphPad Prism (version 5.0; GraphPad Software Inc., San Diego, USA). D'Agostino's K-squared test was used to check data for normality. Multiple comparison of means were undertaken using one-way ANOVA followed by a Tukey's multiple pairwise comparisons test. Results are expressed as mean ± standard error (SE) unless stated. A p-value of < 0.05 was regarded as statistically significant throughout. All experimental runs are paired with relevant controls. The authors acknowledge that as a consequence this can lead to results that can engender substantial variability within the methodology and the controls, however, this also ensures experimental repeats are considered in the context of negative and positive controls.

Results

Effect of hypoxia on EV concentration, size, and size distribution

As Table 1 indicates, hypoxia exposure (1% O_2 – EV^{hypo}) significantly increased CEV production in comparison to CEVs in normoxia (21% O_2 - EV^{norm}) (EV^{hypo}: 1825 ± 72 EVs/cell vs EV^{norm}: 117 ± 9 EVs/cell, $p < 0.001$, respectively). CEV production was significantly reduced following the introduction of nitrite to cells prior to incubation in hypoxia (EV^{hypo+N}: 842 ± 91, $p < 0.001$). However, neither hypoxic conditions, nor the introduction of nitrite, affected EV mean size (EV^{hypo}: 221 ± 6 nm, EV^{norm}: 203 ± 4 nm, EV^{hypo+N}: 211 ± 7 nm, EV^{norm+N}: 206 ± 3, $p > 0.05$).

CEV size distribution was assessed (according to 50 nm bin size), showing EV^{hypo} exhibited an elevated concentration of CEVs at bin size ranges 101-300 nm, and 351-400 nm. The introduction of nitrite to cells incubated in hypoxia reduced the concentration of CEVs versus cells exposed to hypoxia alone at bin size ranges 151-200 nm, 251-300 nm, and 351-400 nm respectively. See Figure 3 for the depiction of CEV size distribution.

	Normoxia		Hypoxia	
	Without NO_2^-	With NO_2^-	Without NO_2^-	With NO_2^-
CEV concentration (EVs/cell)	117 ± 9	123 ± 11	1825 ± 72***	842 ± 91†††
CEV size (nm)	203 ± 4	206 ± 3	221 ± 6	211 ± 7

Table 1. The effect of hypoxia on CEV concentration and size. CEVs were measured using nanoparticle tracking analysis. *** represents $p < 0.001$ compared to normoxia. ††† represents $p < 0.001$ compared to hypoxia without NO_2^-. Results reflect N=5.

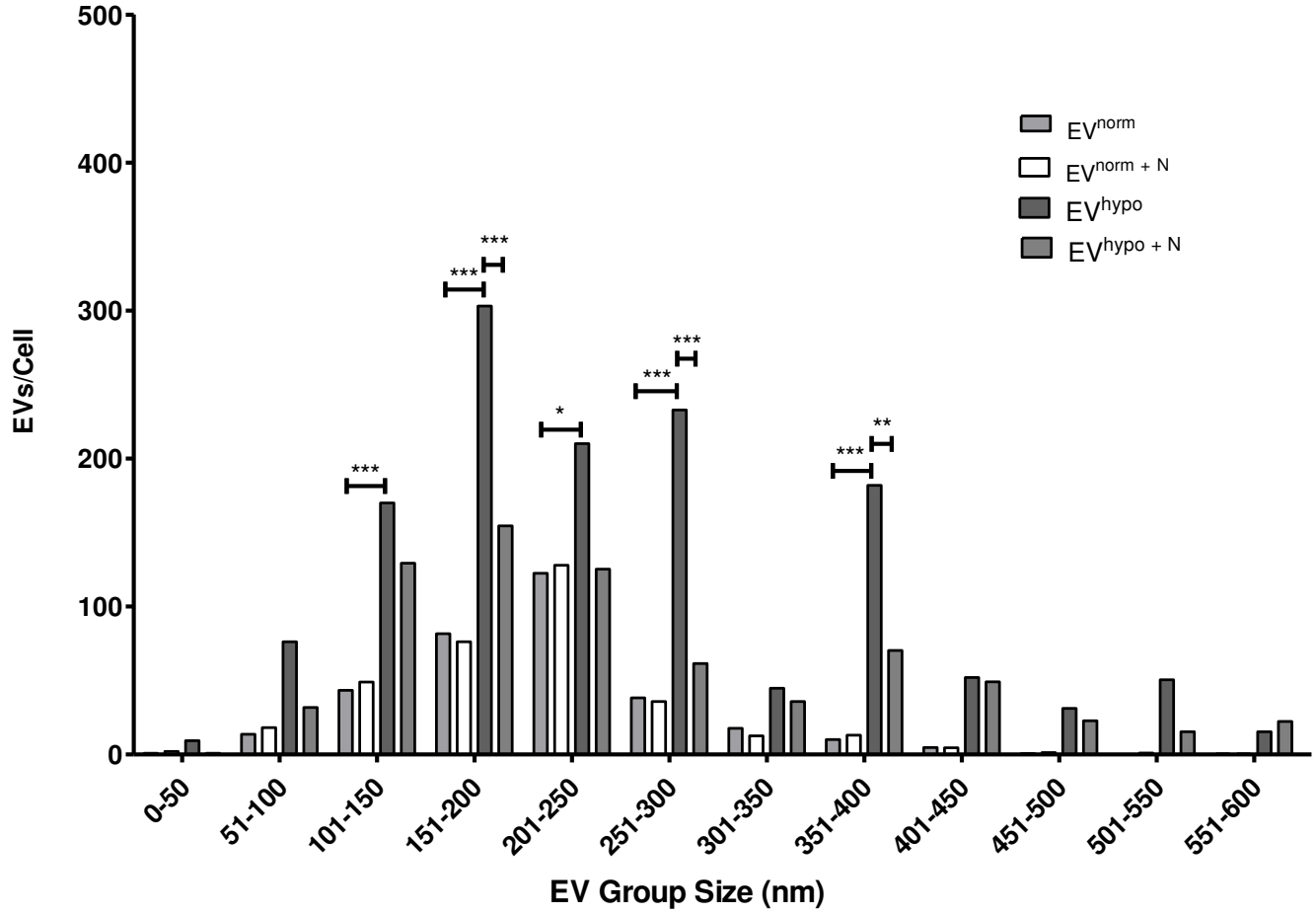

Figure 3. The effect of hypoxia and nitrite on CEV size distribution. CEVs were measured using nanoparticle tracking analysis. Assessed in 50 nm bin sizes, results reflect N=5. EV^{norm} = normoxic EV, EV^{norm+N} = normoxic EV + nitrite, EV^{hypo} = hypoxic EV, EV^{hypo+N} = hypoxic EV + nitrite. ***, ** and * reflect $p < 0.001$, 0.01 and 0.05, respectively.

Characterisation of EVs

HECV are a cell line and as such do not express all the characteristics of primary endothelial cells. We therefore chose to assess the influence of hypoxia and nitrite using primary HUVEC. Like HECVs, hypoxia significantly increases the PEV yield from HUVEC (PEVs/Cell = 1227 ± 50 vs 361 ± 20, $p < 0.001$). Table 2 illustrates that TFPI expression was significantly reduced in EV^{hypo} compared to EV^{norm} (*RFU* = 9799 ± 2353 vs 19723 ± 2698, $p < 0.05$, respectively). The simultaneous addition of NO_2^- to hypoxia-treated HUVECs had no impact on the TFPI expression of the PEVs produced (EV^{hypo+N}) (RFU = 9799 ± 2353). TF expression was significantly elevated in EV^{hypo} and EV^{hypo+N} compared to pre-treatment of HUVECs incubated in normoxia with NO_2^- (EV^{norm+N}) (EV^{hypo}: *RFU* = 7666 ± 1698, EV^{hypo+N}: 9505 ± 1260 vs EV^{norm+N}: 4239 ± 605, $p < 0.001$, respectively). EV^{hypo+N} also expressed significantly higher TF than EV^{norm} (9505 ± 1260 vs 5958 ± 1644, $p < 0.001$). EV^{norm+N} also had no effect on the expression of PEV vWF, TF or TFPI. EV^{norm} and EV^{hypo} exhibited similar levels of the endothelial marker CD144 and the EV associated markers CD9, ALIX, and TSG101 (see Supplementary Data – Figure 2).

	EV^{norm}		EV^{hypo}	
	Without NO_2^-	With NO_2^-	Without NO_2^-	With NO_2^-
vWF	11389 ± 1765	12534 ± 3688	12385 ± 2186	10111 ± 1103
TF	5958 ± 1644	4239 ± 605	7666 ± 1698$^{\zeta}$	9505 ± 1260$^{\zeta\varsigma}$
TFPI	19723 ± 2698	19323 ± 2053	9799 ± 2353*	8524 ± 1084*†

Table 2. Level of coagulation proteins expressed on PEVs. Results are relative fluorescent units (RFU). $^{\zeta}$ represents $p < 0.001$ compared to normoxia with NO_2^-. $^{\varsigma}$ represents $p < 0.001$ compared to normoxia without NO_2^-. * represents $p < 0.05$ compared to normoxia without NO_2^-. † represents $p < 0.05$ compared to normoxia with NO_2^-. Results reflect N=4.

355 **Fluorescent fibrin polymer formation**

356 As displayed by Figures 4A and 4C, fibrin polymer formation was significantly increased
357 following the addition of EV^{norm} to plasma in comparison to control (plasma alone - no CEVs
358 added) (% area = 36.36 ± 0.72 vs. 16.66 ± 1.17, $p < 0.001$, respectively). Similarly, the addition
359 of EV^{hypo} significantly increased the fibrin % area compared to control (% area = 46.98 ± 0.97,
360 $p < 0.001$). The influence of EV^{hypo} was significantly greater than EV^{norm} ($p < 0.01$). Given
361 TFPI regulates the action of the extrinsic coagulation cascade and EV^{hypo} expressed more TF
362 and less TFPI then EV^{Norm}, we investigated if the addition of exogenous TFPI restored fibrin
363 polymerization to the level observed with addition of EV^{norm}. The increased fibrin % area seen
364 following the addition of EV^{hypo} was fully attenuated following the addition of exogenous TFPI
365 in combination with hypoxia-derived EVs ($EV^{hypo+TFPI}$) (19.91 ± 4.91, $p < 0.001$). The addition
366 of TFPI in combination with normoxia-derived EVs had no effect on the fibrin % area (% area
367 = 26.60 ± 0.59, $p > 0.05$). Following the addition of EV^{hypo+N} to plasma, fibrin % area was
368 significantly reduced in comparison to EV^{hypo} (% area = 15.70 ± 1.99 vs 35.97 ± 3.28,
369 respectively, $p < 0.001$). EV^{hypo+N} returned levels to baseline, comparable to EV^{norm}. There was
370 no significant difference between EV^{norm+N} and EV^{norm} (% area = 19.06 ± 2.34 vs 18.59 ± 2.02,
371 respectively, $p > 0.05$). Supplementary Data - Figure 3 illustrates typical formation of fibrin
372 polymers with the addition of normoxia- and hypoxia-derived EVs in the presence and absence
373 of nitrite.
374
375 Figures 4B and 4D compare the number of fibrin strands at each junction. This is a measure of
376 the mechanical strength and hence its resistance to breakdown [48]. The addition of EV^{norm} to
377 plasma significantly reduced strands per junction compared to control plasma (*spj* = 2.93 ±
378 0.05 vs 3.18 ± 0.02, respectively, $p < 0.05$). Following the addition of EV^{norm+N}, strands per
379 junction were reduced further compared to EV^{norm} alone (*spj* = 2.71 ± 0.03 vs 2.93 ± 0.05,
380 respectively, $p < 0.001$). This effect was mirrored by the addition of EV^{hypo+N} compared to
381 EV^{hypo} (*spj* = 2.79 ± 0.04 vs 3.24 ± 0.04, respectively, $p < 0.001$).
382
383
384

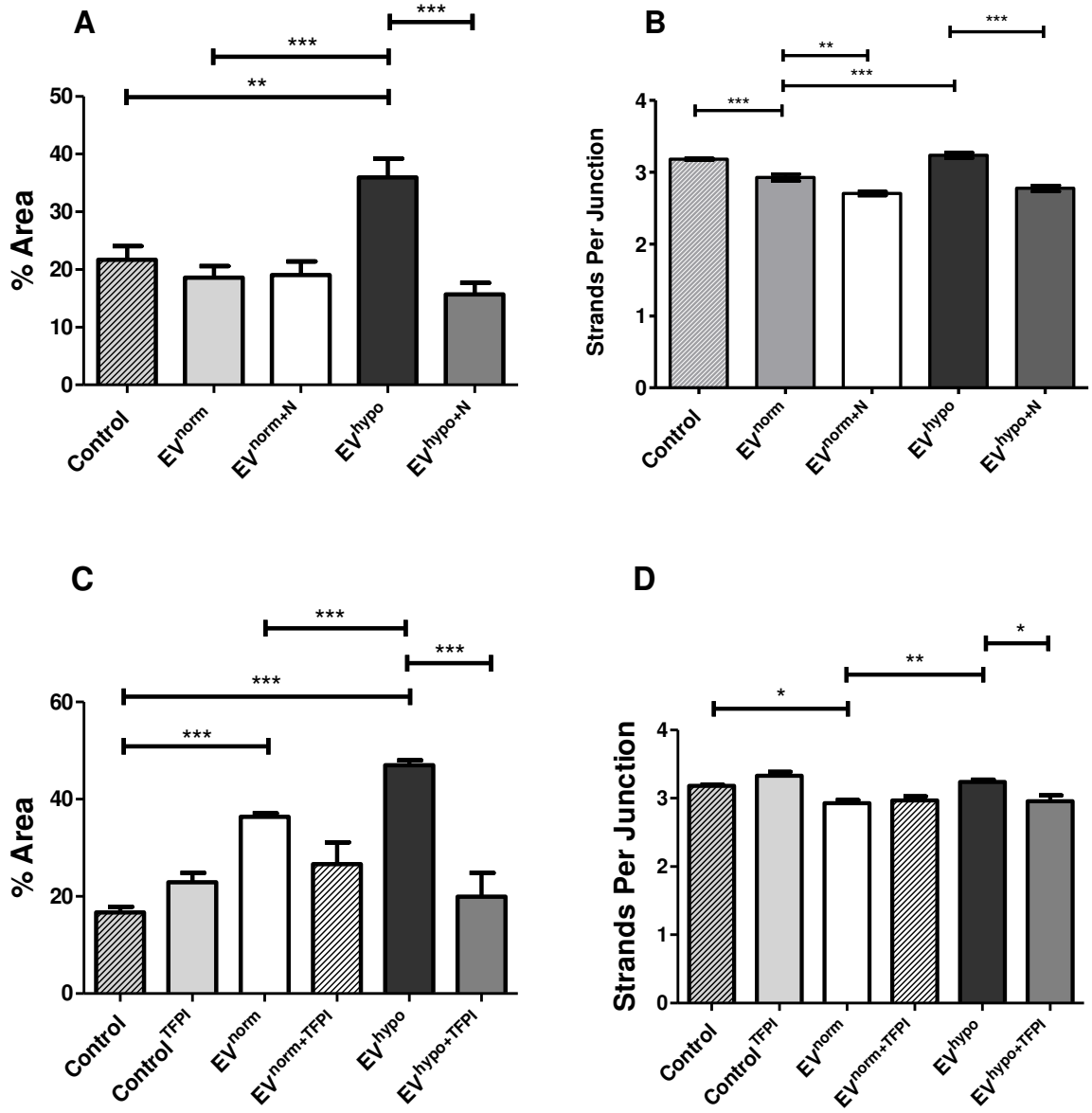

Figure 4. The effect of nitrite and/or TFPI treated CEVs on the contribution to clot formation. CEVs were incubated with platelet poor plasma before clot formation was initiated with a combination of calcium and thrombin. Images were then captured after 15 minutes. **A**. *% Area (EV with NO_2^-)*. **B.** *Strands Per Junction (EV with NO_2^-)*. **C**. *% Area (EV with TFPI)*. **D.** *Strands Per Junction (EV with TFPI)*. EV^{norm} = normoxic EV, EV^{norm+N} = normoxic EV + nitrite, EV^{hypo} = hypoxic EV, EV^{hypo+N} = hypoxic EV + nitrite. Control – Filtered PBS. EVs at concentration 1 x 10^9 EVs. Results represent [N=6]. ***, ** and * reflect $p < 0.001$, 0.01 and 0.05, respectively.

Turbidometry

The maximum optical density (MaxOD), reflecting total clot formed, was greater following addition of CEVs produced under hypoxia compared to normoxia, however this did not reach statistical significance (EV^{norm}: 0.437 ± 0.009 AU, EV^{norm+N}: 0.446 ± 0.015 AU, EV^{hypo}: 0.472 ± 0.007 AU, EV^{hypo+N}: 0.459 ± 0.022 AU, Control: 0.434 ± 0.004 AU, respectively, $p > 0.05$) (Figure 5A).

The time taken for optical density to reach 50% of its MaxOD reflects the rate of clot formation. No significant differences were observed between CEV samples (EV^{norm}: 6.66 ± 0.338 mins, EV^{norm+N}: 6.628 ± 0.417 mins, EV^{hypo}: 6.086 ± 0.482 mins, EV^{hypo+N}: 5.978 ± 0.298 mins, Control: 6.89 ± 0.227 mins, respectively, $p > 0.05$) (Figure 5B). The time taken for the optical density to return to 50% of its MaxOD reflects lysis and is a surrogate for the strength of the clot. In the presence of EV^{hypo} the time to 50% lysis was greater than EV^{norm} however this did not reach statistical significance (EV^{norm}: 8.84 ± 0.471 mins, EV^{norm+N}: 8.4 ± 0.4 mins, EV^{hypo}: 11.4 ± 1.421 mins, EV^{hypo+N}: 10.12 ± 0.913 mins, Control: 8 ± 0.544 mins, $p > 0.05$) (Figure 5C). Similarly, the rate of lysis in the presence of EVs +/- nitrite did not show significant differences (EV^{norm}: -0.030 ± 0.003 AU/min, EV^{norm+N}: -0.034 ± 0.004 AU/min, EV^{hypo}: -0.022 ± 0.004 AU/min, EV^{hypo+N}: -0.028 ± 0.003 AU/min, Control: -0.033 ± 0.003 AU/min, $p > 0.05$) (Figure 5D).

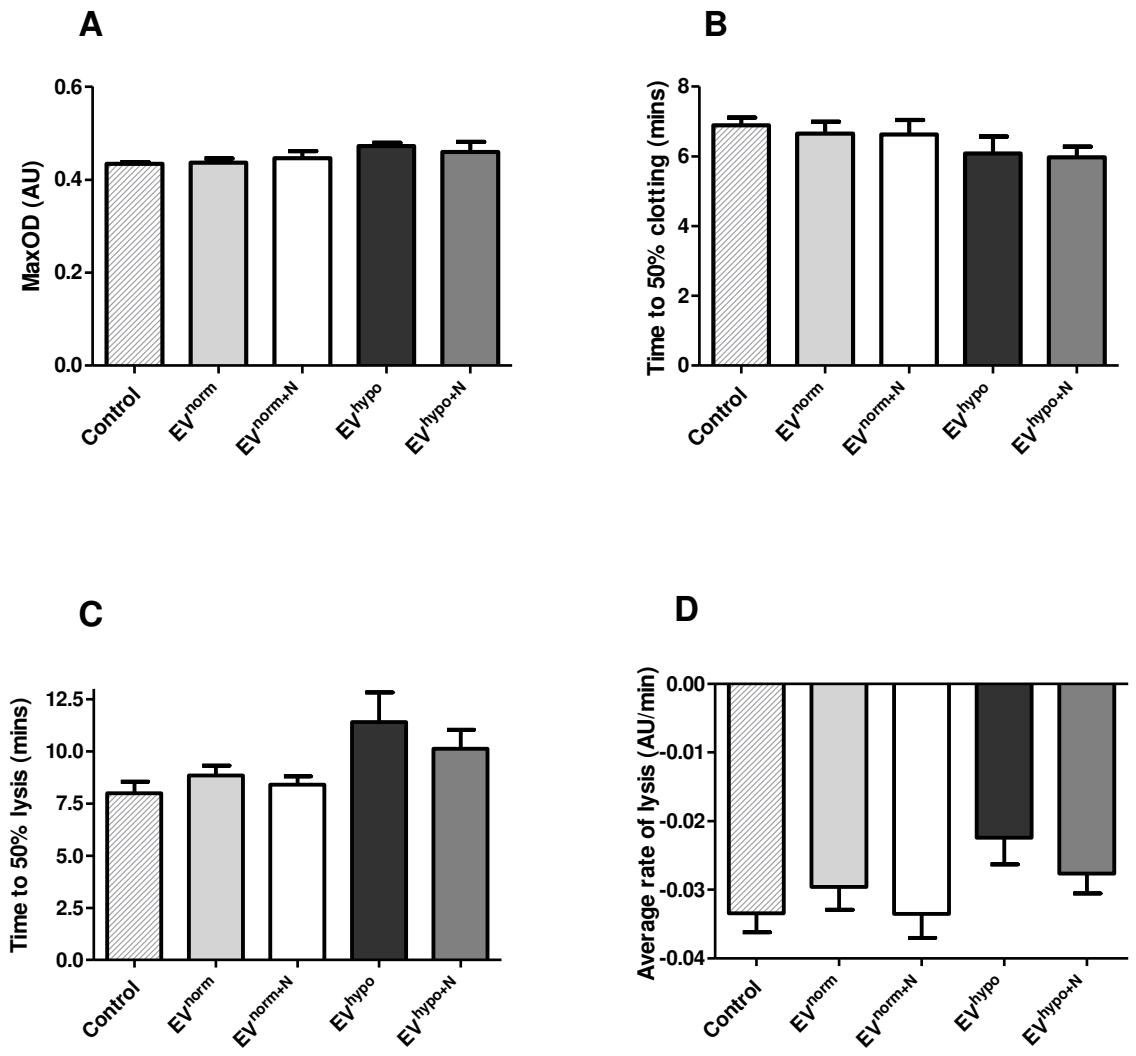

415

416 **Figure 5. The effect of CEVs on thrombin and calcium induced turbidometry.** CEVs were incubated with
417 platelet poor plasma before clot formation was initiated with a combination of calcium and thrombin. **A.**
418 *MaxOD* **B**. *Time to 50% clotting* **C.** *Time to 50% lysis* **D.** *Average rate of lysis*. EV^{norm} = normoxic EV, EV^{norm+N}
419 = normoxic EV + nitrite, EV^{hypo} = hypoxic EV, EV^{hypo+N} = hypoxic EV + nitrite. Control – Filtered PBS.
420 Results reflect [N=5].

421

Platelet activity

Platelet aggregation in response to ADP in the presence of PEV was significantly increased following whole blood incubation with EV^{hypo} compared to control (888.0 ± 32.2 AU*min vs 647.2 ± 38.1 AU*min respectively, $p < 0.01$) (Figure 6A). EV^{hypo} also demonstrated an increase in platelet activity following stimulation by ADP, in comparison to EV^{norm} (671.5 ± 28.3 AU*min, $p < 0.01$) and EV^{norm+N} (616.0 ± 44.9 AU*min, $p < 0.001$). EV^{hypo+N} significantly reduced platelet aggregation in response to ADP compared to EV^{hypo} to levels similar to EV^{norm} (716.5 ± 44.3 AU*min vs 888.0 ± 32.2 AU*min respectively, $p < 0.001$). EV^{norm} and EV^{norm+N} had no effect on platelet activity stimulated via ADP in comparison to control (EV^{norm}: 671.5 ± 28.3 AU*min, EV^{norm+N}: 616.0 ± 44.9 AU*min, control: 647.2 ± 38.1 AU*min, $p > 0.05$).

Following stimulation with TRAP in the presence of PEV, EV^{hypo} increased platelet aggregation in comparison to EV^{norm} (922.2 ± 30.1 AU*min vs 641.2 ± 25.2 AU*min, $p < 0.05$) (Figure 6B). EV^{hypo+N} significantly reduced platelet aggregation compared to EV^{hypo} (650.3 ± 45.4 AU*min vs 922.2 ± 30.1 AU*min respectively, $p < 0.05$). EV^{norm+N} had no effect on platelet aggregation compared to EV^{norm} (612.3 ± 115.2 AU*min vs 641.2.0 ± 25.2 AU*min respectively, $p > 0.05$).

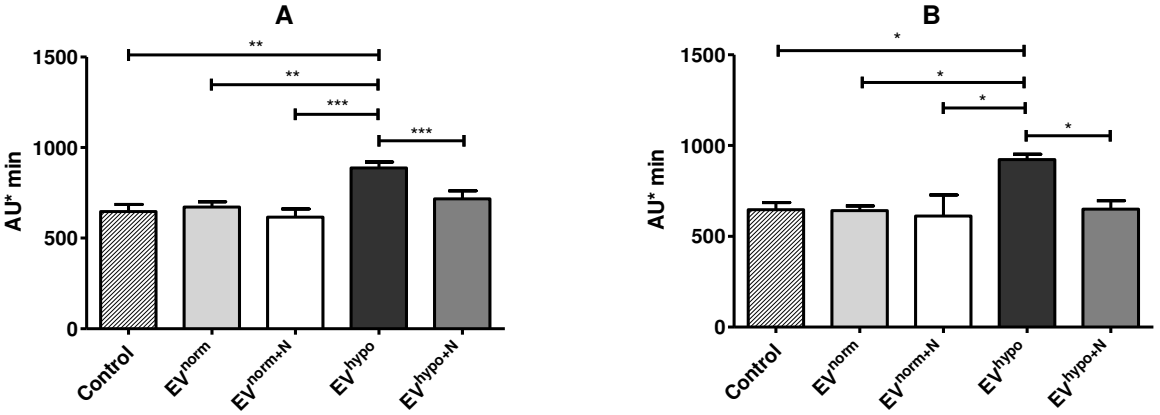

Figure 6. The effect of PEVs on ADP- and TRAP- mediated platelet aggregation. PEVs were incubated with whole blood, before platelets were stimulated with either ADP **(A)** or TRAP **(B)**. Aggregation units calculated as area under the curve after 6 minutes (impedance:time). EV^{norm} = normoxic EV, EV^{norm+N} = normoxic EV + nitrite, EV^{hypo} = hypoxic EV, EV^{hypo+N} = hypoxic EV + nitrite. Control – Filtered PBS. Results represent [N=6]. ***, ** and * reflect p < 0.001 and 0.01 and 0.05, respectively.

Fractal Dimension and Clot Formation Time

To corroborate the findings of the plasma fibrinogen assay in a whole blood assay, fractal dimension (d_f) and clot formation time (T_{GP}) were measured in the presence and absence of PEV produced under various conditions. d_f was significantly elevated following the addition of EV^{hypo} to whole blood, in comparison to control (d_f = 1.03 ± 0.0067 vs 1.00 ± 0.00, respectively, $p < 0.001$) (Figure 7A). EV^{hypo} also significantly increased d_f in whole blood in comparison to EV^{norm} and EV^{norm+N} (d_f= EV^{hypo}: 1.030 ± 0.0067, EV^{norm}: 1.012 ± 0.0029, EV^{norm+N}: 1.007 ± 0.0027, $p < 0.05$ and $p < 0.01$ respectively). Interestingly, EV^{hypo+N} significantly reduced d_f in comparison to EV^{hypo} alone, to similar levels seen with EV^{norm} (d_f = 1.005 ± 0.0017 vs 1.012 ± 0.0029 respectively, $p < 0.001$). d_f was not significantly different between EV^{norm} and control (d_f = 1.012 ± 0.0030 vs 1.00 ± 0.00 respectively, $p > 0.05$). EV^{norm+N} had no influence on d_f in comparison to EV^{norm} (d_f = 1.007 ± 0.0026 vs 1.012 ± 0.0030, respectively, $p > 0.05$).

T_{GP} was significantly reduced by EV^{norm} in comparison to control (T_{GP} = 221.4 ± 19.71 seconds vs 273.4 ± 12.31 seconds respectively, $p < 0.05$) (Figure 7B). EV^{norm+N} increased T_{GP} in comparison to EV^{norm} (T_{GP} = 278.6 ± 7.78 secs vs 221.4 ± 19.71 secs respectively, $p < 0.05$). EV^{hypo} significantly reduced T_{GP} in comparison to control (T_{GP} =181.6 ± 8.98 seconds vs 273.4 ± 12.31 seconds respectively, $p < 0.05$). Interestingly, EV^{hypo} did not significantly alter T_{GP} in comparison to EV^{norm} (T_{GP} = 181.6 ± 8.98 seconds vs 221.4 ± 19.71 seconds respectively, $p > 0.05$). EV^{hypo+N} appeared to reverse the effect of EV^{hypo} on T_{GP}, with EV^{hypo+N} restoring T_{GP} to a similar level as the control (T_{GP} = EV^{hypo+N}: 250.8 ± 4.2 seconds vs EV^{hypo}: 181.6 ± 8.99 seconds, $p < 0.01$).

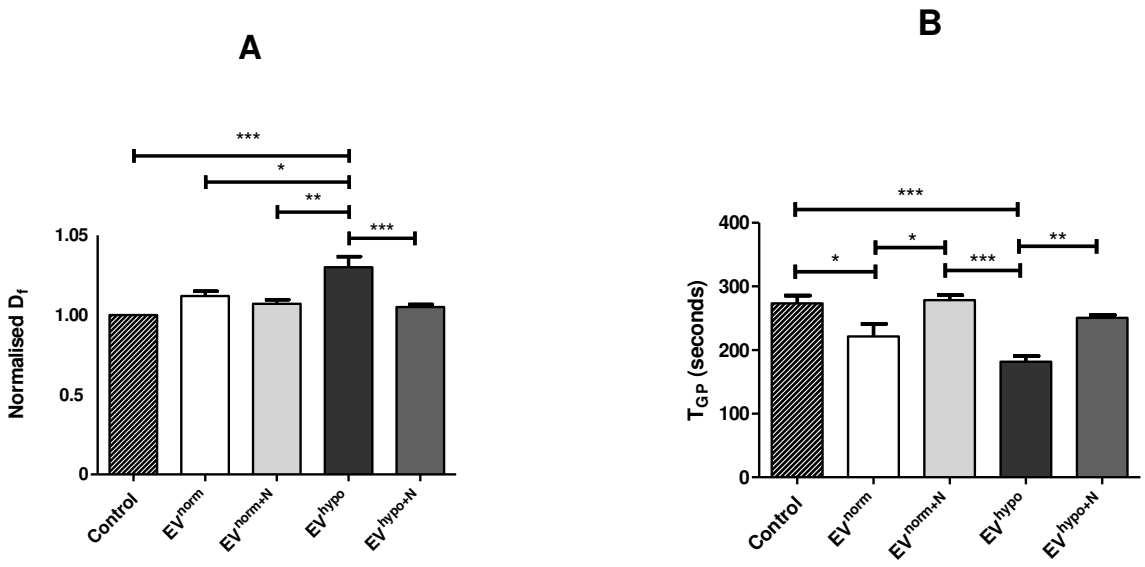

Figure 7. The effect of hypoxia and nitrite treated PEVs on fractal dimension (d_f) and clot formation time (T_{GP}). A. EVs were added to whole blood and incubated for 15 minutes form, in seconds. Results are normalised to an EV-free PBS control, and represent mean ± standard error. EV^{norm} = normoxic EV, EV^{norm+N} = normoxic EV + nitrite, EV^{hypo} = hypoxic EV, EV^{hypo+N} = hypoxic EV + nitrite. Control – EV-free filtered PBS. **B**. T_{GP} represents the time taken for a blood clot to EVs. d_f results are normalised to the EV-free control. Results represent [N=5]. ***, ** and * reflect $p < 0.001$, 0.01 and 0.05, respectively.

497

498 **Thrombin activity**

499 Thrombin activity was measured in the plasma of healthy volunteers and was not affected by
500 the presence of EV^{norm} in comparison to control (128.9 ± 4.2 ng/mL vs 114.6 ± 15.6 ng/mL
501 respectively, $p > 0.05$) (Figure 8). EV^{norm+N} did not alter thrombin activity compared to EV^{norm}
502 (EV^{norm+N}:131.6 ± 9.5 ng/mL vs EV^{norm}: 128.9 ± 4.2 ng/mL, $p > 0.05$). EV^{hypo} significantly
503 increased thrombin activity in comparison to both EV^{norm} and EV^{norm+N} (EV^{hypo}: 187.1 ± 14.8
504 ng/mL, EV^{norm}: 128.9 ± 4.2 ng/mL, EV^{norm+N}: 131.6 ± 9.5 ng/mL, $p < 0.05$). EV^{hypo+N} did not
505 significantly reduce thrombin activity in comparison to EV^{hypo} (190.7 ± 18.1 ng/mL vs 187.1 ±
506 14.8 ng/mL, respectively). EV^{hypo+N} significantly increased thrombin activity in comparison to
507 EV^{norm} and EV^{norm+N} (EV^{hypo+N}: 190.7 ± 18.1 ng/mL, EV^{norm}: 128.9 ± 4.2 ng/mL, EV^{norm+N}:
508 131.6 ± 9.5 ng/mL, $p < 0.05$).

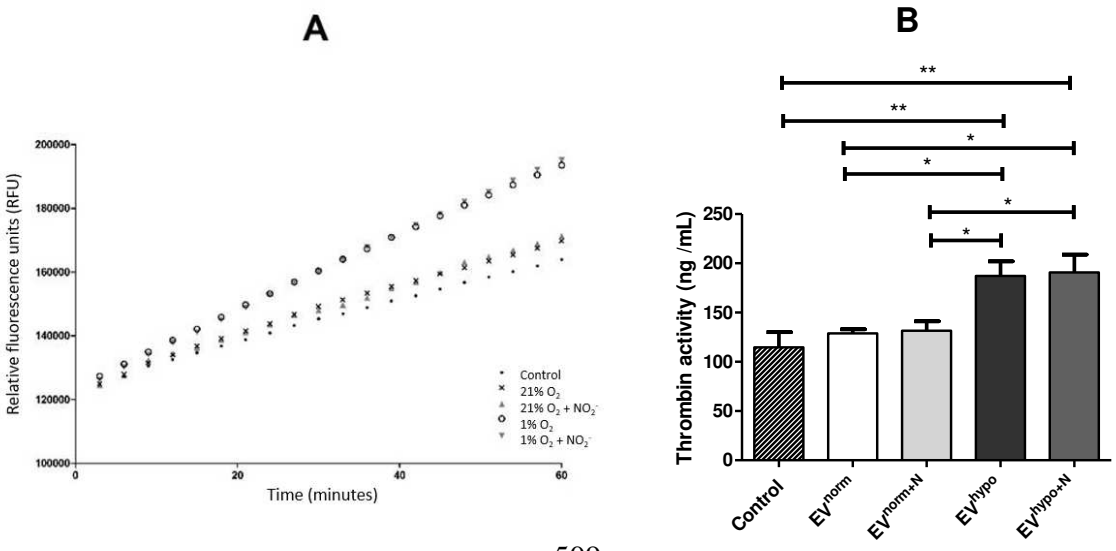

509

510 **Figure 8. The effect of PEVs on thrombin activity. A.** Thrombin generation was measured in the plasma of
511 healthy volunteers incubated with EVs over the course of 60 minutes. **B**. Thrombin activity was then calculated,
512 using a standard curve of known thrombin concentration. EV^{norm} = normoxic EV, EV^{norm+N} = normoxic EV +
513 nitrite, EV^{hypo} = hypoxic EV, EV^{hypo+N} = hypoxic EV + nitrite. Control – Filtered PBS. Results reflect [N=8] **
514 and * reflect $p < 0.05$ and 0.01, respectively.

Electron microscopy

Scanning electron microscopy highlighted structural differences in fibrin clots produced following whole blood incubation with PEV isolated from various conditions (Figure 9). The addition of PEV appeared to lead to direct incorporation into the fibrin clot, with multiple sub-micron particles visibly attached to the fibres, largely absent in the control (no EV added). Qualitatively, clots formed in the presence of EV^{hypo} and EV^{hypo+N} appear denser and more compact. EV^{norm+N} appeared to reduce the density of the clot in comparison to EV^{norm}, a finding consistent with the quantitative fibrin clot formation assay and fractal dimension results.

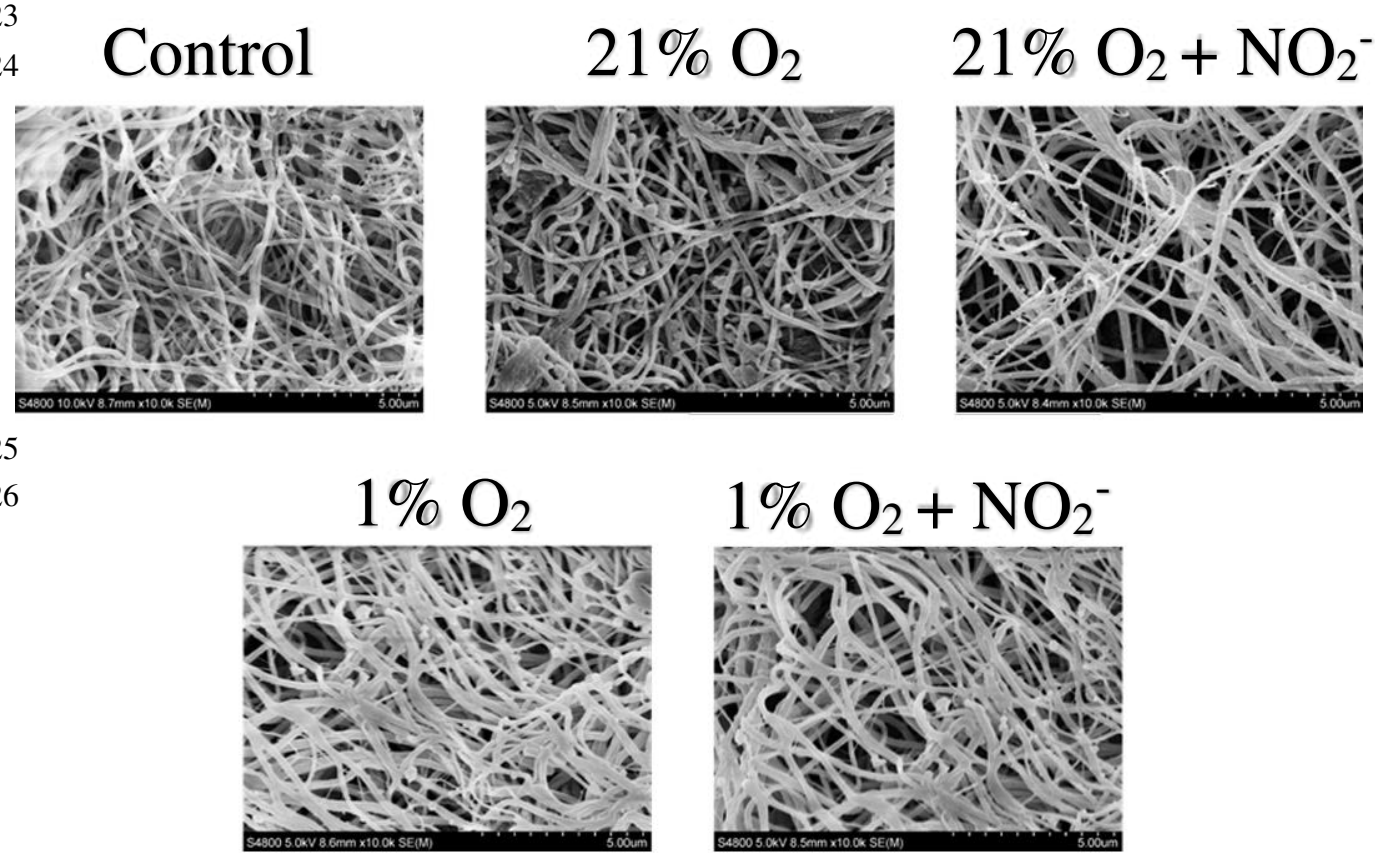

Figure 9. Typical scanning electron micrographs of fibrin clots. PEV appear to be incorporated within the fibrin network. Control – Filtered PBS added to whole blood. The magnification bar is 5 µm for all images, shown in 500 nm increments.

Discussion

This study demonstrates that endothelial cell-derived EV production is markedly increased under hypoxic conditions, and these EV exhibit pro-coagulant characteristics and function under normal conditions in comparison to endothelial EVs derived from normoxia. The mechanism appears to be mediated by an imbalance in TF/TFPI content of hypoxia-derived EVs. Pre-incubation of hypoxic HUVECs with inorganic NO_2^- abrogated the ability of the PEVs to exert their pro-coagulant effect measured in three separate model systems of clot formation.

The mechanical properties of blood clots are essential for homeostasis and the prevention of blood loss. However, clots composed of compact fibrin strands are more resistant to lysis, and can predispose individuals to arterial thrombotic events [48–52]. Indeed, alterations in clot structure have been implicated in various thrombotic diseases, including ischemic stroke [48,51], heart failure [52] and coronary artery disease [53,54]. The structural composition of the clot defines its fibrinolytic properties, with a compact, tight fibrin network reducing the penetration of fibrinolytic components. Conversely, a loose structure with thick fibres is more susceptible to lysis due to high plasmin penetration of fibrinolytic components [55, 56].

EVs derived from platelets and endothelial cells form an intrinsic part of clot formation and stability. Consistent with this, our data in three separate model systems shows endothelial EVs generated under hypoxic conditions exhibit increased pro-coagulative capacity when tested under normal conditions. Significant increases in fibrin polymerisation were induced on addition of EV^{hypo} to plasma. This effect was abrogated when plasma was incubated with EV^{hypo+N}, confirming that NO_2^- is capable of modulating the character of EVs produced under hypoxic conditions. EV^{norm} and EV^{norm+N} had no effect on fibrin polymerisation in comparison to control. Platelet aggregation in whole blood was also elevated in response to the agonists ADP and TRAP when pre-incubated with EV^{hypo}, whilst addition of NO_2^- to cells alleviated this effect, regardless of the agonist used for stimulation. Thus, NO_2^- appears to protect against the generation of pro coagulant, hypoxic CEVs. This was further confirmed using fractal dimension (d_f) and clot formation time (T_{GP}) in whole blood. A significant relationship has

previously been observed between the SEM of fibrin clots and d_f, whereby a higher df was associated with highly dense clots formed of smaller fibrin fibres [57,58].

We also show that EV^{hypo} elevated thrombin production significantly. However, NO_2^- pre-treatment of cells had no effect on thrombin generating capacity of EV^{hypo}. On examination of the biogenic cargo of the PEVs, NO_2^- had no effect on levels of vWF, TF, thrombomodulin or TFPI, suggesting the NO_2- effect is independent of the presence of these mediators of the coagulation cascade.

Qualitatively, scanning electron microscopy revealed EV^{hypo} promoted the formation of a more compact, denser clot in comparison to EV^{norm}, which may imply greater resistance to subsequent fibrinolysis. This is consistent with our findings of adding EV^{hypo} in our fluorescent fibrin assay and d_f analysis. Previous work by Weisel *et al* has shown that platelet-derived EVs attach to fibrin and incorporate themselves within the clot network [59]. Consistent with this, we observed that EV treatment leads to the incorporation of spherical particles 200-500 nm in size into the fibrin clot that are largely absent in the controls.

Prior to clot activation we observed only diffuse fluorescence (fibrinogen) which became visible as fibrin strands only when incorporated into the fibrin polymer network stimulated by thrombin (see Supplementary Figure 3). Interestingly, even in the absence of hypoxia, pre-incubation of endothelial cells with NO_2^- resulted in CEVs that significantly reduced the number of fibrin strands per junction, compared to controls, implying NO_2^- can reduce the pro-coagulant effect of normoxic CEV. NO_2^- at a concentration similar to that which was used in our own study [59-63] is thought to elicit its vasoprotective effects via reduction to "NOx" species, a pathway that is significantly enhanced during hypoxia. *In vivo,* there is certainly evidence that NO_2^- may also elicit its effects via hypoxia-independent mechanisms involving the formation of a nitrosothiol (RSNO) [64,65]. Feelisch *et al* [66] have recently shown that NO_2^- induces delayed and long-lasting blood pressure lowering effects even in normoxia via an NO-independent mechanism involving redox intermediates. Importantly, in the present studies NO_2^- (30μM) was added to cells in culture and the resulting EVs harvested via multiple ultracentrifugation steps. To confirm little carry over of NO_2^- into our functional assays, ozone-based chemiluminescence detection of NO_2^- [67] showed levels typically <100nM. Furthermore, addition of NO_2^- at 30μM directly to plasma without CEV had no effect on fibrin strand formation. In order to test for differential metabolism of NO_2^- by endothelial cells in

normoxia compared to hypoxia, we measured nitrite and nitrate by ozone based chemiluminescence and observed a relatively small 2.82μM and 1.61μM decrease in NO_2^-, respectively (N=3). This indicates overall reduced nitrite metabolism under hypoxic conditions. The authors are careful not to over interpret this result, since we had predicted the overall nitrite/nitrate concentration would remain unchanged. This was based on the fact production of NO from NO_2^- under hypoxic conditions will ultimately lead to products that are relatively unstable and will ultimately re-cycle back to nitrite and nitrate that are detected by ozone-based chemiluminescence in the cell culture medium. However, in our experience studies undertaken to recover nitrite/nitrate from cell culture based experiments are fraught with difficulty including the sampling time point and the stability of multiple products formed. The importance of NO_2^- reduction and involvement of NO in control of EV generation by endothelial cells under hypoxic conditions has previously been confirmed [20]. Approximately 60% of NO_2^- reduction is attributable to xanthine oxidoreductase activity at 1% O_2, as shown by co-treatment with Allopurinol (100μM). Furthermore, the importance of nitrite reduction to NO in hypoxia in the context of inhibiting the stability of HIF-1α and induction of EV production (as opposed to a direct effect of nitrite on HIF-1) is also evident from our previous finding that addition of nitrite to cells co-treated with the hypoxia mimetic agent Desferrioxamine (100μM) under normoxic conditions so as to induce HIF had no effect on typical "hypoxia" mediated increases in EV.

Hypoxia has been shown to induce changes in several proteins in cells involved in coagulation via HIF-1, including upregulation of TF [68] and PAI-1 [24], and downregulation of thrombomodulin [69] and TFPI [70]. Our immunoassay results suggest that EV^{hypo} reflect the composition of their parent cells; with significant reductions in TFPI levels compared to EV^{norm}. The addition of exogenous TFPI to the assay in combination with EV^{hypo} to plasma, resulted in a significant reduction in total fibrin polymerisation compared to EV^{hypo} alone, confirming EV^{hypo} exhibit their pro-coagulant effect primarily through the extrinsic pathway of the coagulation cascade. Taken together with the finding that EV^{hypo} also express increased levels of TF compared to EV^{norm}, the imbalance in TF/TFPI can result in increased TF-FVII complex formation, activation of factor Xa and ultimately, enhanced fibrin polymerization. The effect of endothelial EVs under different culture conditions on the coagulation cascade is summarised in Figure 10.

Previous studies have shown that hypoxia-derived EVs express increased TF [71-73]. In agreement with this, EV^{hypo} expressed increased TF in the presence and absence of nitrite. HIFs are capable of repressing transcription of genes such as TFPI by directly binding to the hormone response element (HRE) [22], as shown previously in breast cancer cells where inhibition of HIF-1α reversed the effects of hypoxia on TFPI expression [70]. There is also evidence to suggest HIF may also regulate TF expression, however this is yet to be fully elucidated [73,74]. Interestingly, a previous study identified an imbalance between TF and TFPI within circulating EVs in individuals with Behçet's Syndrome and concluded this may predispose these individuals to thrombosis [75].

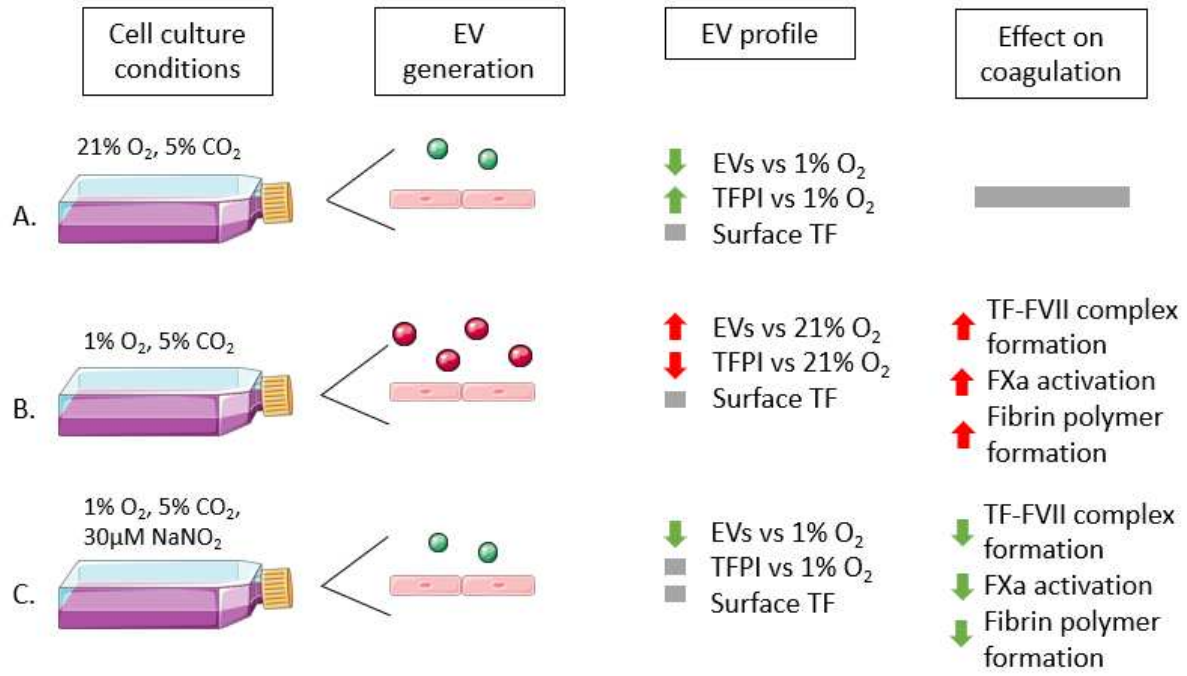

Figure 10. Summary of the influence of oxygen concentration on EV generation and EV-mediated coagulation. A. EVs isolated from cells conditioned in 21% O_2. B. EVs isolated from cells conditioned in 1% O_2. C. EVs isolated from cells conditioned in 1% O_2, pre-conditioned with $NaNO_2$. Green EV represent EV high in TFPI, whereas red EV represent EV with low TFPI.

On examination of the biogenic cargo of the EVs, NO_2^- had no effect on levels of vWF, TF or TFPI, suggesting the inhibitory effects of NO_2^- observed are independent of EV supply of these mediators of the coagulation cascade. The high level of pro-coagulant phosphatidylserine (PS) exposure on the surface of EVs can also provide a negatively charged surface for formation of the prothrombinase complex [76], mediated by the calcium-dependent floppase and scramblase

membrane bound enzymes [77]. Since NO elicits many of its effects, including modulation of platelet activation and vasodilation, via a reduction in intracellular calcium [78], it is reasonable to suggest NO_2^- could act via a similar mechanism. In addition, we have previously observed that treatment of endothelial cells with NO_2^- under hypoxic conditions abrogates the hypoxia-induced increase in EV number via its destabilising effects on HIF-1α. Since PS exposure on the cell membrane is a critical step in EV generation, it is reasonable to predict that the effects of NO_2^- on PS exposure might be linked to its effects on HIF-1α under hypoxic conditions [20]. This remains to be confirmed.

The pathological role of endothelial EV within cardiovascular disease, specifically coagulation, is well established [79,80]. Clinically, the role of hypoxia in stimulating endothelial EV in the context of acute ischaemic stroke [81] and myocardial infarction [82, 83] is now recognised. Extrapolating the results from this study to *in vivo*, modulation of the pro-thrombotic character of hypoxia derived endothelial EV by increasing NO_2^- availability may prove beneficial in patients at risk of thrombotic events. Our group have previously shown increases in plasma NO_2^- and RSNO (via an acute dietary nitrate supplement) in CAD patients can reduce circulating plasma EV, coupled with a reduction in platelet aggregation [16], studies which need replicating in large patient cohorts.

An important limitation of these studies is we chose to focus on a NO_2^- dose of 30μM based upon the maximal inhibition effect of NO_2^- on EV production [20]. This is significantly higher than typical baseline nitrite concentration observed in plasma. However, we are keen to point out when exogenous nitrite is given to subjects (either directly in the form of an infusion or indirectly in the form of dietary nitrate such as beetroot), plasma nitrite peak reaches low μM ranges of NO_2^- in healthy subjects (reviewed in [84]). Nevertheless, it is important to point out 30μM represents a supra-physiological level and these studies are proof of principle. A further limitation is we chose 1% O_2 as an in vitro model of tissue ischaemia. We had previously shown that HIF is expressed at O_2 concentrations <2% [20] and we have applied this model extensively to mimic in vivo hypoxia associated with ischaemia. This is consistent with the concept that hypoxia in cell culture models is considered to be below 5% O_2 [85]. It also agrees with the work of Mann *et al* [86] who have studied the concept of "Physioxia" extensively and suggest between 3-13% O_2 best represents

true physiological conditions in an in vitro setting (depending on the cell type) whereas below this should be termed “Hypoxia”.

In summary, this study highlights the pro-coagulant potential of hypoxia-derived endothelial-EVs and confirms this to be mediated by an imbalance in EV TF/TFPI content. Pre-incubation of endothelial cells in hypoxia with NO_2^- alleviated the pro-coagulant effect of the resulting EV, however, the mechanism was independent of TF/TFPI and appears to be mediated by the de-stabilizing effect of NO (from NO_2^-) on HIF-1α. Future studies should further elucidate the mechanisms by which NO_2^- modulates the biogenic cargo and subsequent function of pro-coagulant EVs.

Conflict of Interests

None declared.

Acknowledgements

The authors would like to thank Miss Vanessa Evans and Dr Matthew Lawrence (School of Medicine, Swansea University) for their technical support and assistance with the electron microscopy and running the d_f samples.

Funding

This work was partly funded by a Health and Care Research Wales Scholarship awarded to NBH.

Supplemental Data

Fluorescent fibrin polymer formation

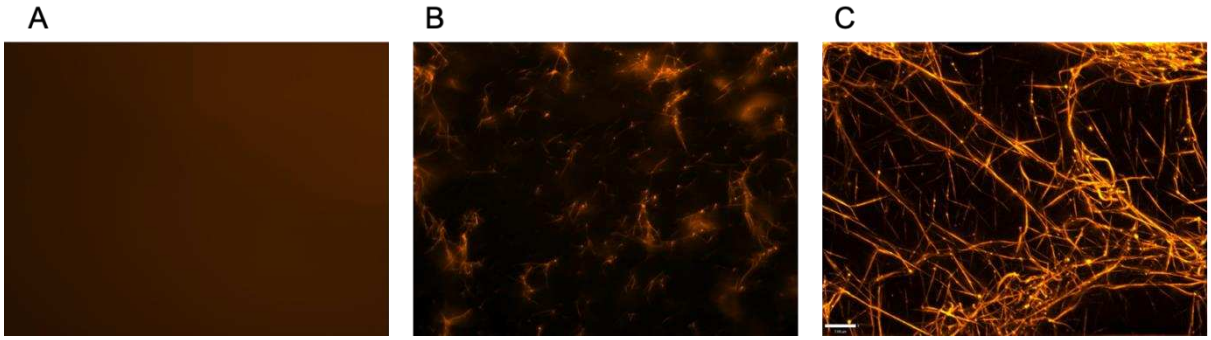

Figure 1. Image capture of fluorescently labelled fibrin polymer formation over 15 minutes. A – represents 5 minutes post clot activation using thrombin and $CaCl_2$. **B** – captured 10 minutes post activation. **C** – captured 15 minutes post activation and used to perform the analysis on. Images captured at 100x magnification. This is based on modification of a previously established assay [41].

Characterisation of EVs

EVs derived from all conditions displayed similar levels of exosomal (CD9, ALIX, TSG101) and endothelial (CD144) markers, with no significant differences observed between groups (Figure 2).

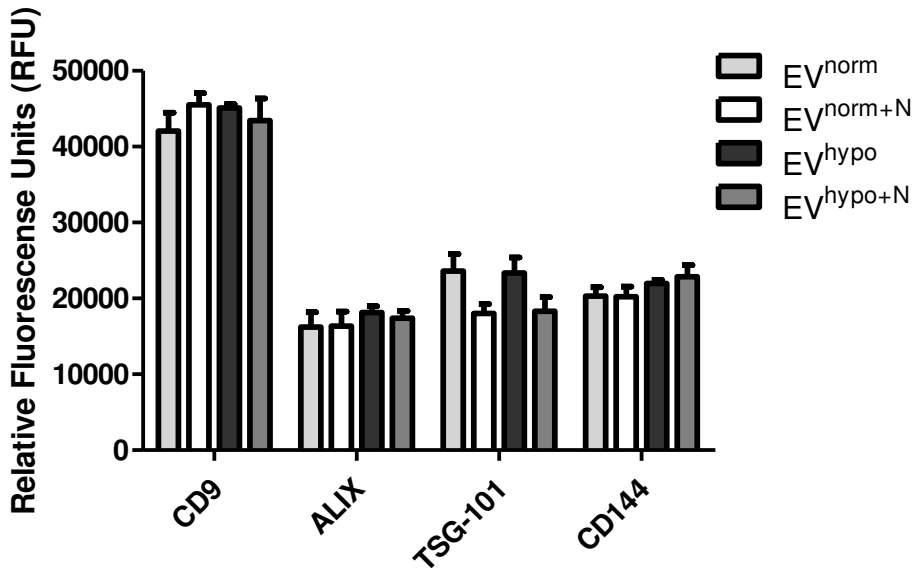

Figure 2. Character of PEVs incubated in hypoxia ± nitrite. EV, exosomal and endothelial marker levels. EV^{norm} = normoxic EV, EV^{norm+N} = normoxic EV + nitrite, EV^{hypo} = hypoxic EV, EV^{hypo+N} = hypoxic EV + nitrite. Results reflect N=4. * reflects $p < 0.05$.

Fluorescent fibrin polymer formation

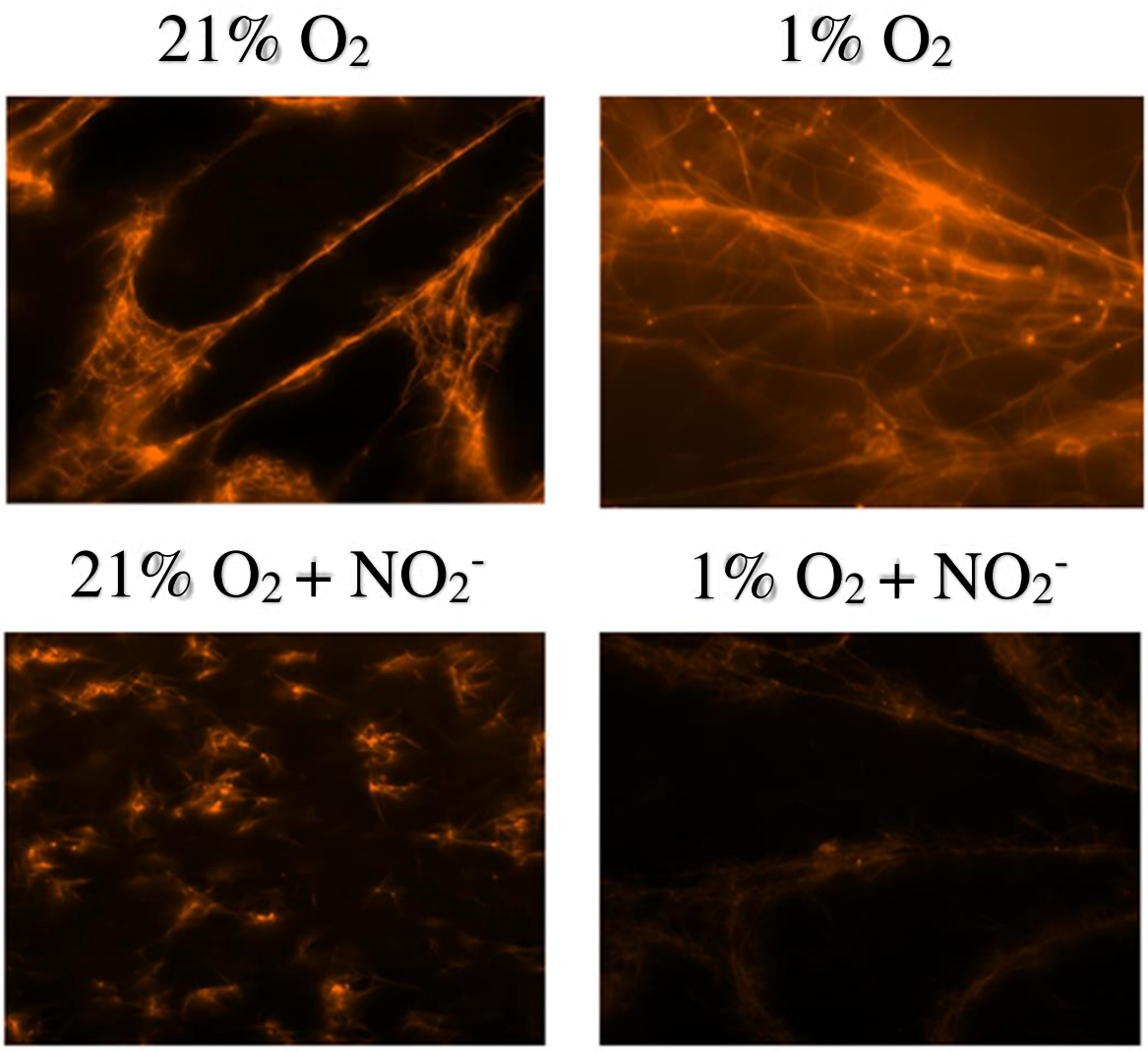

Figure 3. Typical images captured following the formation of fibrin polymers with the addition of CEVs. Combined image overlay of activated clot with the addition of an EV subgroup. Captured 15 minutes post clot activation using a 488nm laser at 100x magnification.

References

1. Mulcahy LA, Pink RC, Carter DRF. Routes and mechanisms of extracellular vesicle uptake. *J Extracell Vesicles*; 2014; **3**: 24641.

2. van der Pol E, Böing AN, Harrison P, Sturk A, Nieuwland R. Classification, functions, and clinical relevance of extracellular vesicles. *Pharmacol Rev*; 2012; **64**: 676–705.

3. Wendler F, Favicchio R, Simon T, Alifrangis C, Stebbing J, Giamas G. Extracellular vesicles swarm the cancer microenvironment: from tumor–stroma communication to drug intervention. *Oncogene*; 2017; **36(7)**: 877–84.

4. D'Souza-Schorey C, Clancy JW. Tumor-derived microvesicles: shedding light on novel microenvironment modulators and prospective cancer biomarkers. *Genes Dev*; 2012; **26(12)**: 1287–99.

5. Yamada N, Kuranaga Y, Kumazaki M, Shinohara H, Taniguchi K, Akao Y. Colorectal cancer cell-derived extracellular vesicles induce phenotypic alteration of T cells into tumor-growth supporting cells with transforming growth factor-β1-mediated suppression. *Oncotarget*; 2016; **7(19)**: 27033.

6. Bellingham SA, Guo B, Coleman B, Hill AF. Exosomes: Vehicles for the Transfer of Toxic Proteins Associated with Neurodegenerative Diseases? *Front Physiol*. 2012; **0**: 124.

7. Schneider A, Simons M. Exosomes: vesicular carriers for intercellular communication in neurodegenerative disorders. *Cell Tissue Res*; 2013; **352(1)**: 33–47.

8. Vella LJ, Sharples RA, Nisbet RM, Cappai R, Hill AF. The role of exosomes in the processing of proteins associated with neurodegenerative diseases. *Eur Biophys J*; 2007; **37(3)**: 323–32.

9. Thompson AG, Gray E, Heman-Ackah SM, Mäger I, Talbot K, Andaloussi S El, et al. Extracellular vesicles in neurodegenerative disease — pathogenesis to biomarkers. *Nat Rev Neurol*; 2016; **12(6)**: 346–57.

10. Horstman LL, Jy W, Jimenez JJ, Ahn YS. Endothelial microparticles as markers of endothelial dysfunction. *Front Biosci*; 2004; **9**: 1118–35.

11. Gaceb A, Martinez MC, Andriantsitohaina R. Extracellular vesicles: New players in cardiovascular diseases. *Int J Biochem Cell Biol*; 2014; **50(1)**: 24–8.

12. VanWijk MJ, VanBavel E, Sturk A, Nieuwland R. Microparticles in cardiovascular diseases. *Cardiovasc Res*; 2003; **59(2)**: 277–87.

13. Dignat-George F, Boulanger CM. The many faces of endothelial microparticles. *Arterioscler Thromb Vasc Biol*; 2011; **31(1)**:27–33.

14. Markiewicz M, Richard E, Marks N, Ludwicka-Bradley A. Impact of endothelial microparticles on coagulation, inflammation, and angiogenesis in age-related vascular diseases. *Journal of Aging Research*; 2013; **2013**: 734509.

15. Rautou P-E, Vion A-C, Amabile N, Chironi G, Simon A, Tedgui A, et al. Microparticles, Vascular Function, and Atherothrombosis. *Circ Res*. 2011; **109(5)**: 593–606.

16. Burnley-Hall N, Abdul F, Androshchuk V, Morris K, Ossei-Gerning N, Anderson R, et al. Dietary Nitrate Supplementation Reduces Circulating Platelet-Derived Extracellular Vesicles in Coronary Artery Disease Patients on Clopidogrel Therapy: A Randomised, Double-Blind, Placebo-Controlled Study. *Thromb Haemost*; 2018; **118(1)**:112–22.

17. Pichler Hefti J, Leichtle A, Stutz M, Hefti U, Geiser T, Huber AR, et al. Increased endothelial microparticles and oxidative stress at extreme altitude. *Eur J Appl Physiol*; 2016; **116(4)**: 739–48.

18. Michiels C. Physiological and pathological responses to hypoxia. *Am J Pathol American Society for Investigative Pathology*; 2004; **164**: 1875–82.

19. Ziello JE, Jovin IS, Huang Y. Hypoxia-Inducible Factor (HIF)-1 regulatory pathway and its potential for therapeutic intervention in malignancy and ischemia. Yale Journal of Biology and Medicine. *Yale Journal of Biology and Medicine*; 2007; **80**: 51–60.

20. Burnley-Hall N, Willis G, Davis J, Rees DA, James PE. Nitrite-derived nitric oxide reduces hypoxia-inducible factor 1α-mediated extracellular vesicle production by endothelial cells. Nitric Oxide; 2017; 63: 1–12.

21. de Jong OG, Verhaar MC, Chen Y, Vader P, Gremmels H, Posthuma G, et al. Cellular stress conditions are reflected in the protein and RNA content of endothelial cell-derived exosomes. *J Extracell Vesicles*; 2012; **1(1)**: 18396.

22. Stavik B, Espada S, Cui XY, Iversen N, Holm S, Mowinkel M-C, Halvorsen B, Skretting G, Sandset PM. EPAS1/HIF-2 alpha-mediated downregulation of tissue factor pathway inhibitor leads to a pro-thrombotic potential in endothelial cells. *Biochim Biophys Acta - Mol Basis Dis;* 2016; **1862**: 670–8.

23. Seigneur M, Dufourcq P, Belloc F, Lenoble M, Renard M, Boisseau MR. Influence of pentoxifylline on membrane thrombomodulin levels in endothelial cells submitted to hypoxic conditions. *J Cardiovasc Pharmacol*; 1995; **25 Suppl 2**: S85-7.

24. Görlach A, Berchner-Pfannschmidt U, Wotzlaw C, Cool RH, Fandrey J, Acker H, Jungermann K, Kietzmann T. Reactive oxygen species modulate HIF-1 mediated PAI-1 expression: involvement of the GTPase Rac1. *Thromb Haemost*; 2003; **89**: 926–35.

25. Kucharzewska P, Christianson HC, Welch JE, Svensson KJ, Fredlund E, Ringnér M, Mörgelin M, Bourseau-Guilmain E, Bengzon J, Belting M. Exosomes reflect the hypoxic status of glioma cells and mediate hypoxia-dependent activation of vascular cells during tumor development. *Proc Natl Acad Sci U S A National Academy of Sciences*; 2013; **110**: 7312–7.

26. Göhner C, Schlembach D, Schleussner E, Markert UR, Fitzgerald JS. PP009. Hypoxia alters syncytiotrophoblastic microparticles (STBM)-related coagulation capacities. *Pregnancy Hypertens An Int J Women's Cardiovasc Heal*; 2013; **3**: 70.

27. Yokota N, Koizume S, Miyagi E, Hirahara F, Nakamura Y, Kikuchi K, Ruf W, Sakuma Y, Tsuchiya E, Miyagi Y. Self-production of tissue factor-coagulation factor VII complex by ovarian cancer cells. *Br J Cancer*; 2009; **101**: 2023–9.

28. Bidot L, Jy W, Bidot C, Jimenez JJ, Fontana V, Horstman LL, Ahn YS. Microparticle-mediated thrombin generation assay: increased activity in patients with recurrent thrombosis. *J Thromb Haemost*; 2008; **6**: 913–9.

29. Srihirun S, Sriwantana T, Unchern S, Kittikool D, Noulsri E, Pattanapanyasat K, Fucharoen S, Piknova B, Schechter AN, Sibmooh N. Platelet Inhibition by Nitrite Is Dependent on Erythrocytes and Deoxygenation. *PLoS One*; 2012; **7**: 30380.

30. Maher AR, Milsom AB, Gunaruwan P, Abozguia K, Ahmed I, Weaver RA, Thomas P, Ashrafian H, Born GVR, James PE, Frenneaux MP. Hypoxic Modulation of Exogenous Nitrite-Induced Vasodilation in Humans. *Circulation*; 2008; **117**: 670–7.

31. Velmurugan S, Gan JM, Rathod KS, et al. Dietary nitrate improves vascular function in patients with hypercholesterolemia: a randomized, double-blind, placebo-controlled study. Am J Clin Nutr 2016; **103**: 25–38.

32. Velmurugan S, Kapil V, Ghosh SM, et al. Antiplatelet effects of dietary nitrate in healthy volunteers: involvement of cGMP and influence of sex. Free Radic Biol Med 2013; **65**: 1521–32.

33. Metzen E, Zhou J, Jelkmann W, Fandrey J, Brüne B. Nitric Oxide Impairs Normoxic Degradation of HIF-1α by Inhibition of Prolyl Hydroxylases; *Journal of Cellular and Molecular Medicine*; 2003; **14(8)**: 3470–81.

34. Wang J-M, Wang Y, Huang J-Y, Yang Z, Chen L, Wang L-C, et al. C-Reactive Protein-Induced Endothelial Microparticle Generation in HUVECs Is Related to BH4-Dependent NO Formation. *J Vasc Res*; 2007; **44(3)**: 241–8.

35. Park JW, Piknova B, Nghiem K, Lozier JN, Schechter AN. Inhibitory effect of nitrite on coagulation processes demonstrated by thrombelastography. *Nitric Oxide - Biol Chem*; 2014; **40**: 45–51.

36. Park JW, Piknova B, Huang PL, Noguchi CT, Schechter AN. Effect of Blood Nitrite and Nitrate Levels on Murine Platelet Function. *PLoS One*; 2013; **8**: 2.

37. Srihirun S, Sriwantana T, Unchern S, Kittikool D, Noulsri E, Pattanapanyasat K, et al. Platelet inhibition by nitrite is dependent on erythrocytes and deoxygenation. *PLoS One*; 2012; **7**: 1.

38. Crampton SP, Davis J, Hughes CCW. Isolation of human umbilical vein endothelial cells (HUVEC). *Journal of Visualized Experiments*; 2007; **3**: 183.

39. Webber J, Clayton A. How pure are your vesicles? *J Extracell Vesicles*; 2013; **2(1)**.

40. Connolly KD, Guschina IA, Yeung V, Clayton A, Draman MS, Von Ruhland C, Ludgate M, James PE, Rees DA. Characterisation of adipocyte-derived extracellular vesicles released pre- and post-adipogenesis. *J Extracell vesicles*; 2015; **4**: 29159.

41. Weiss N, Schenk B, Bachler M, Solomon C, Fries D, Hermann M. FITC-linked Fibrin-Binding Peptide and real-time live confocal microscopy as a novel tool to visualize fibrin(ogen) in coagulation. *J Clin Transl Res*; 2017; **3(2)**: 76–82.

42. Sakharov, D. v., Barrertt-Bergshoeff, M., Hekkenberg, R. T., & Rijken, D. C. Fibrin-specificity of a plasminogen activator affects the efficiency of fibrinolysis and responsiveness to ultrasound: comparison of nine plasminogen activators in vitro. *Thrombosis and Haemostasis*; 1999; ***81*(4)**, 605–612.

43. Schneider, P. C., & Clegg, R. M. Rapid acquisition, analysis, and display of fluorescence lifetime-resolved images for real-time applications. *Review of Scientific Instruments*; 1999; ***68*(11)**, 4107.

44. Carter, A. M., Cymbalista, C. M., Spector, T. D., & Grant, P. J. Heritability of clot formation, morphology, and lysis: The EuroCLOT study. *Arteriosclerosis, Thrombosis, and Vascular Biology*; 2012; ***27*(12)**, 2783–2789.

45. Hooper, J. M. W., Stuijver, D. J. F., Orme, S. M., van Zaane, B., Hess, K., Gerdes, V. E., Phoenix, F., Rice, P., Smith, K. A., Alzahrani, S. H., Standeven, K. F., & Ajjan, R. A. (2012). Thyroid Dysfunction and Fibrin Network Structure: A Mechanism for Increased Thrombotic Risk in Hyperthyroid Individuals. *The Journal of Clinical Endocrinology & Metabolism;* 2012*; **97*(5)**, 1463–1473.

46. Evans PA, Hawkins K, Morris RHK, Thirumalai N, Munro R, Wakeman L, Lawrence MJ, Williams PR. Gel point and fractal microstructure of incipient blood clots are significant new markers of hemostasis for healthy and anticoagulated blood. *Blood;* 2010; **116**: 3341–6.

47. Lawrence MJ, Kumar S, Hawkins K, Boden S, Rutt H, Mills G, Sabra A, Morris RHK, Davidson SJ, Badiei N, Brown MR, Williams PR, Evans PA. A new structural biomarker that quantifies and predicts changes in clot strength and quality in a model of progressive haemodilution. *Thromb Res;* 2014; **134**: 488–94.

48. Pera J, Undas A, Topor-Madry R, Jagiella J, Klimkowicz-Mrowiec A, Slowik A. Fibrin Clot Properties in Acute Stroke: What Differs Cerebral Hemorrhage From Cerebral Ischemia? *Stroke*; 2012; **43**: 1412–4.

49. Weisel JW. BIOPHYSICS: Enigmas of Blood Clot Elasticity. *Science*; 2008; **320**: 456–7.

50. Undas A, Ariens RAS. Fibrin Clot Structure and Function: A Role in the Pathophysiology of Arterial and Venous Thromboembolic Diseases. *Arterioscler Thromb Vasc Biol*; 2011; **31**: 88–99.

51. Undas A, Zawilska K, Ciesla-Dul M, Lehmann-Kopydlowska A, Skubiszak A, Ciepluch K, Tracz W. Altered fibrin clot structure/function in patients with idiopathic venous thromboembolism and in their relatives. *Blood*; 2009; **114**: 4272–8.

52. Undas A, Podolec P, Zawilska K, Pieculewicz M, Jedlinski I, Stepien E, Konarska-Kuszewska E, Weglarz P, Duszynska M, Hanschke E, Przewlocki T, Tracz W. Altered Fibrin Clot Structure/Function in Patients With Cryptogenic Ischemic Stroke. *Stroke*; 2009; **40**: 1499–501.

867 53. Palka I, Nessler J, Nessler B, Piwowarska W, Tracz W, Undas A. Altered fibrin clot properties in patients
868 with chronic heart failure and sinus rhythm: a novel prothrombotic mechanism. *Heart*; 2010; **96**: 1114–8.

869 54. Neergaard-Petersen S, Hvas A-M, Kristensen SD, Grove EL, Larsen SB, Phoenix F, Kurdee Z, Grant PJ,
870 Ajjan RA. The influence of type 2 diabetes on fibrin clot properties in patients with coronary artery disease.
871 *Thromb Haemost*; 2014; **112**: 1142–50.

872 55. Sabra A, Lawrence MJ, Aubrey R, Obaid D, Chase A, Smith D, Thomas P, Storton S, Davies GR, Hawkins
873 K, Williams PR, Morris K, Evans PA. Characterisation of clot microstructure properties in stable coronary
874 artery disease. *BMJ*; 2017; **4**.

875 56. Colle JP, Mishal Z, Lesty C, Mirshahi M, Peyne J, Baumelou A, Bensman A, Soria J, Soria C. Abnormal
876 fibrin clot architecture in nephrotic patients is related to hypofibrinolysis: influence of plasma biochemical
877 modifications: a possible mechanism for the high thrombotic tendency? *Thromb Haemost*; 1999; **82**: 1482–9.

878 57. Silveira A, Hamsten A. Fibrin Gel Architecture Influences Endogenous Fibrinolysis and May Promote
879 Coronary Artery Disease. *Arterioscler Thromb Vasc Biol*; 2006; **26**: 2419–20.

880 58. Davies, N. A., Harrison, N. K., Keith Morris, R. H., Noble, S., Lawrence, M. J., D'Silva, L. A., Broome, L.,
881 Brown, M. R., Hawkins, K. M., Williams, P. R., Davidson, S., & Evans, P. A. Fractal dimension (df) as a new
882 structural biomarker of clot microstructure in different stages of lung cancer. *Thrombosis and Haemostasis*;
883 2017; ***114*(6)**, 1251–1259.
884
885 59. Zubairova LD, Nabiullina RM, Nagaswami C, Zuev YF, Mustafin IG, Litvinov RI, Weisel JW. Circulating
886 Microparticles Alter Formation, Structure, and Properties of Fibrin Clots. *Sci Rep*; 2015; **5**: 17611.
887
888 60. Maher AR, Milsom AB, Gunaruwan P, Abozguia K, Ahmed I, Weaver RA, Thomas P, Ashrafian H, Born
889 GVR, James PE, Frenneaux MP. Hypoxic Modulation of Exogenous Nitrite-Induced Vasodilation in Humans.
890 *Circulation*; 2008; **117**: 670–7.
891
892 61. Zhang Z, Naughton D, Winyard PG, Benjamin N, Blake DR, Symons MC. Generation of nitric oxide by a
893 nitrite reductase activity of xanthine oxidase: a potential pathway for nitric oxide formation in the absence of
894 nitric oxide synthase activity. *Biochem Biophys Res Commun*; 1998; **249**: 767–72.
895
896 62. Lundberg JO, Weitzberg E, Gladwin MT. The nitrate-nitrite-nitric oxide pathway in physiology and
897 therapeutics. *Nat Rev Drug Discov*; 2008; **7**: 156–67.
898
899 63. Ingram TE, Fraser AG, Bleasdale RA, Ellins EA, Margulescu AD, Halcox JP, et al. Low-dose sodium nitrite
900 attenuates myocardial ischemia and vascular ischemia-reperfusion injury in human models. *J Am Coll Cardiol*.
901 2013; **61(25)**: 2534–41.
902

64. Pinheiro LC, Amaral JH, Ferreira GC, Portella RL, Ceron CS, Montenegro MF, Toledo JC, Tanus-Santos JE. Gastric S-nitrosothiol formation drives the antihypertensive effects of oral sodium nitrite and nitrate in a rat model of renovascular hypertension. *Free Radic Biol Med*; 2015; **87**: 252–62.

65. Anderson RA, Bundhoo S, James PE. A new mechanism of action of thienopyridine antiplatelet drugs - a role for gastric nitrosthiol metabolism? *Atherosclerosis*; 2014; **237**: 369–73.

66. Feelisch M, Akaike T, Griffiths K, Ida T, Prysyazhna O, Goodwin JJ, et al. Long-lasting blood pressure lowering effects of nitrite are NO-independent and mediated by hydrogen peroxide, persulfides, and oxidation of protein kinase G1α redox signalling. *Cardiovasc Res*; 2020; **116(1)**: 51–62.

67. Pinder AG, Rogers SC, Khalatbari A, Ingram TE, James PE. The measurement of nitric oxide and its metabolites in biological samples by ozone-based chemiluminescence. *Methods Mol Biol*. 2008; **476**: 11–28.

68. Monteiro RQ, Lima LG, Gonçalves NP, DE Souza MRA, Leal AC, Demasi MAA, Sogayar MC, Carneiro-Lobo TC. Hypoxia regulates the expression of tissue factor pathway signaling elements in a rat glioma model. *Oncol Lett Spandidos Publications*; 2016; **12**: 315–22.

69. Dufourcq P, Seigneur M, Pruvost A, Dumain P, Belloc F, Amiral J, Boisseau MR. Membrane thrombomodulin levels are decreased during hypoxia and restored by cAMP and IBMX. *Thromb Res*; 1995; **77**: 305–10.

70. Cui XY, Tinholt M, Stavik B, Dahm AEA, Kanse S, Jin Y, Seidl S, Sahlberg KK, Iversen N, Skretting G, Sandset PM. Effect of hypoxia on tissue factor pathway inhibitor expression in breast cancer. *J Thromb Haemost*; 2016; **14**: 387–96.

71. Abid Hussein M, Böing A, Biró É, Hoek F, Vogel G, Meuleman D, Sturk A, Nieuwland R. Phospholipid composition of in vitro endothelial microparticles and their in vivo thrombogenic properties. *Thrombosis Research*; 2008; **121(6)**, 865-871.

72. Monteiro RQ, Lima LG, Gonçalves NP, DE Souza MRA, Leal AC, Demasi MAA, Sogayar MC, Carneiro-Lobo TC. Hypoxia regulates the expression of tissue factor pathway signaling elements in a rat glioma model. *Oncol Lett*; 2016; **12**: 315–22.

73. Collier M, Mah PM, Xiao Y, Maraveyas A, Ettelaie C. Microparticle-associated tissue factor is recycled by endothelial cells resulting in enhanced surface tissue factor activity. *Blood Coagulation, Fibrinolysis, and Cellular Haemostasis*; 2013; **110**: 966-976.

74. Yan SF, Zou YS, Gao Y, Zhai C, Mackman N, Lee SL, Milbrandt J, Pinsky D, Kisiel W, Stern D. Tissue factor transcription driven by Egr-1 is a critical mechanism of murine pulmonary fibrin deposition in hypoxia. *Proc Natl Acad Sci U S A*; 1998; **95**: 8298–303.

75. Khan E, Ambrose NL, Ahnström J, Kiprianos AP, Stanford MR, Eleftheriou D, et al. A low balance between microparticles expressing tissue factor pathway inhibitor and tissue factor is associated with thrombosis in Behçet's Syndrome. *Sci Rep*; 2016; **6(1)**: 1–12.

941 76. Lentz BR. Exposure of platelet membrane phosphatidylserine regulates blood coagulation. *Prog Lipid Res*;
942 2003; **42**: 423–38.

943 77. Hankins HM, Baldridge RD, Xu P, Graham TR. Role of Flippases, Scramblases and Transfer Proteins in
944 Phosphatidylserine Subcellular Distribution. *Traffic*; 2015; **16**: 35–47.

945 78. Loscalzo J, Welch G. Nitric oxide and its role in the cardiovascular system. *Prog Cardiovasc Dis*; 1994; **38**:
946 87–104.

947 79. Markiewicz M, Richard E, Marks N, Ludwicka-Bradley A. Impact of endothelial microparticles on
948 coagulation, inflammation, and angiogenesis in age-related vascular diseases. *J Aging Res*; 2013; **2013**: 734509.

949 80. Dignat-George F, Boulanger CM. The many faces of endothelial microparticles. *Arterioscler Thromb Vasc*
950 *Biol*; 2011; **31**: 27–33.

951 81. Chiva-Blanch G, Suades R, Crespo J, Peña E, Padró T, Jiménez-Xarrié E, et al. Microparticle Shedding from
952 Neural Progenitor Cells and Vascular Compartment Cells Is Increased in Ischemic Stroke. Combes V, editor.
953 *PLoS One*. 2016; **11(1).**

954 82. Sahoo S, Losordo DW. Exosomes and cardiac repair after myocardial infarction. *Circ Res*. 2014; **114(2)**:
955 333–44.

956 83. Yuan MJ, Maghsoudi T, Wang T. Exosomes Mediate the Intercellular Communication after Myocardial
957 Infarction. *Int J Med Sci*. 2016; **13(2)**: 113–6.

958 84. James PE, Willis GR, Allen JD, Winyard PG, Jones AM. Nitrate pharmacokinetics: Taking note of the
959 difference. *Nitric Oxide*. 2015; **48**: 44-50

960 85. Al-Ani A, Toms D, Kondro D, Thundathil J, Yu Y, Ungrin M. Oxygenation in cell culture: Critical
961 parameters for reproducibility are routinely not reported. PLoS One. 2018; **13(10)**: e0204269.

962 86. Warpsinski G, Smith MJ, Srivastava S, Keeley TP, Siow RCM, Fraser PA, Mann GE. Nrf2-regulated redox
963 signaling in brain endothelial cells adapted to physiological oxygen levels: Consequences for sulforaphane
964 mediated protection against hypoxia-reoxygenation. Redox Biol. 2020; **37**: 101708.

965

966

967

968

969